2023

Effect of Decorating Super Paramagnetic Iron Oxide Nanoparticles with Silver Nanoparticles on their Magneto-Photo Thermal Heating Efficiency

Anthony Joseph Afful
Minnesota State University, Mankato

Recommended Citation

Effect of Decorating Super Paramagnetic Iron Oxide Nanoparticles

with Silver Nanoparticles on Their Magneto-Photo Thermal

Heating Efficiency

by

Anthony Joseph Afful

A thesis submitted in partial fulfilment of the requirements for the Master of

Science in Physics at Minnesota State University, Mankato.

Minnesota State University, Mankato

July, 2023

Endorsement Page

Date of Approval:_____

Title: Effect of Decorating Super Paramagnetic Iron Oxide Nanoparticles with Silver

Nanoparticles on Their Magneto-Photo Thermal Heating Efficiency

Author: Anthony Joseph Afful

This thesis has been examined and approved by the following members of

the students committee:

_____

Dr. Maheshika Palihawadana

_____

Dr. Andy Roberts

_____

Dr. Andrew Clough

_____

Dr. Jorge Mendéz

Acknowledgements

Effect of Decorating Super Paramagnetic Iron Oxide Nanoparticles with

Silver Nanoparticles on Their Magneto-Photo Thermal Heating Efficiency

ABSTRACT BODY

 Cancer treatment is rather dangerous to the body, often involving many secondary

effects, including nausea, hair loss, and weight fluctuations. The search for non-invasive,

highly efficient, and targetable treatments ameliorates these issues. Super paramagnetic

iron oxide nanoparticles (SPIONS) have been used for other medical purposes such as

magnetic resonance imaging contrast agent and is being extensively studied as a potential

candidate for many cancer therapeutic and diagnostic approaches due to its

biocompatibility and superior magnetic properties. When subjected to an external

alternating magnetic field SPIONS generate heat mainly due to the friction of the

SPIONS against the fluid it is suspended in. Upon exposure to this magnetic heating, at

the temperatures about 42-45°C, cancer cells have reduced viability than the healthy

cells. SPIONs show promising properties for being a localized magnetic hyperthermia

treatment agent. There are limitations in this approach, however. When interacting with

cell structures the magnetic heating effect is diminished. To overcome this, alterations to

the SPIONS are sought out. In this study SPIONS, and SPIONS decorated with a photo

thermal agent, Silver, were successfully synthesized and characterized. The dual heating

approaches, magnetic and Photothermal, are tested on the SPIONS and Ag-SPIONS in

hopes of achieving bimodal therapy. Additionally, conventional synthesis methods versus

green methods will be investigated.

Contents

List of Figures

Table of Tables

Chapter 1: Introduction

1.1 Cancer

Treating cancer has been an ongoing concern since 3000 BC when it was first discovered. Various amounts of effort (with varying degrees of efficacy) have been made throughout the history of medicine with more recent attempts becoming increasingly targeted and sophisticated. With the introduction of biocompatible nanotechnology, we are on a new forefront of being able to treat this disease of the cell. With cancer rates predicted to rise[i], finding new methods to treat cancer are important.

Cancer occurs when a cell has reproduced in an abnormal manner and continues to grow uncontrollably[ii]. Removing or otherwise preventing the tissue from reproducing is the primary mode of treating this disease. The current methods such as chemotherapy, removal of organs, and radiation while better than nothing, do often come with intense side effects.
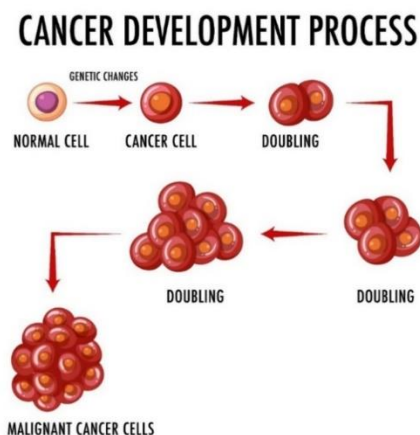
Figure 1: Diagram outlining the rapid growth process of cancer cells[iii].

Since cancer cells tend to grow fast, chemo drugs are designed to kill fast-growing cells. Due to the way they function chemo drugs travel throughout the body where they interact with healthy cells that are fast-growing. The resulting damage to healthy cells causes side effects. These include fatigue, nausea, hair loss, anemia, and fertility problems. The healthy cells most often damaged by chemo are blood-forming cells in the bone marrow, hair follicles, cells in the mouth, digestive tract, and reproductive system. Additionally, chemo drugs can damage cells in the heart, kidneys, bladder, lungs, and nervous system[iv]. For radiation therapy the side effects often include general damaging or weakening of the selected area including rib fractures if the thoracic cavity is the target area. For the heart it increases the risk of heart disease. Generally, the bombardment of the area with high energy particles damages the healthy tissue[v].

1.2 Nano Particles and Cancer Therapy

Nano particles are particles that range in size from a few to several hundred nanometers (10^{-9} m). Nanotechnology is the field concerning their intentional usage to achieve specific goals. Their physical characteristics often bridge the gap between behaviors at the atomic and molecular level and bulk materials, once a certain amount of the material is present. Their usages vary from drug delivery, pathogen detection, DNA reading, and tissue alteration, just to name a few[vi]. There are many different types of nanoparticles that are being investigated for various biomedical applications as shown in Figure 2:
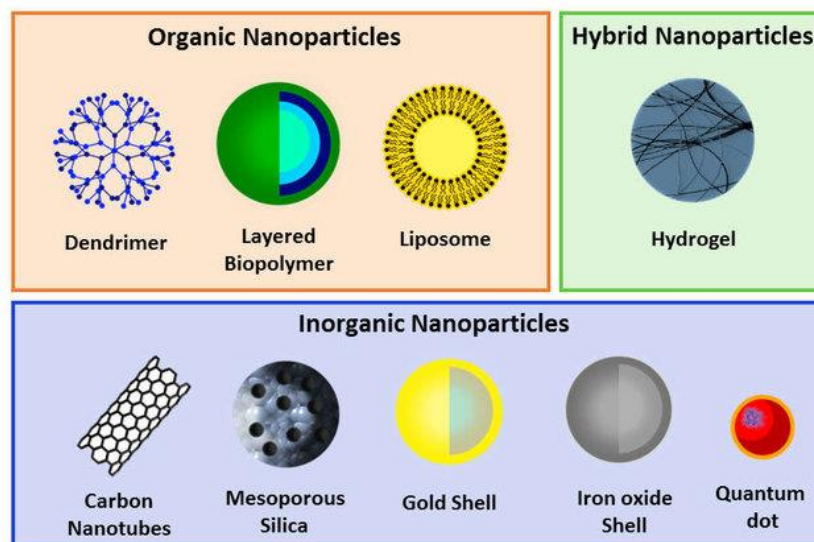
Figure 2: Diagram showing the different types of nanoparticles used in biomedical applications[vii].

In recent years, studies on magnetic nanoparticles (MNPs) have been dramatically increasing for usage in cancer therapy and diagnostic (also known as theranostic) applications due to their unique physical and chemical properties, magnetic resonance imaging (MRI) contrast, facile synthesis, easy surface decorations, low toxicity, and good biodegradability. These characteristics assist them to serve as outstanding imaging agents, and delivery vehicles in cancer theranostics[viii]. Being magnetically responsive, they also can be delivered to specific sites within the body and are excellent for localized usage and treatment. To date, MNPs have been developed from nickel, cobalt, Prussian Blue, and gadolinium. Iron oxide, however, has been the most extensively studied.
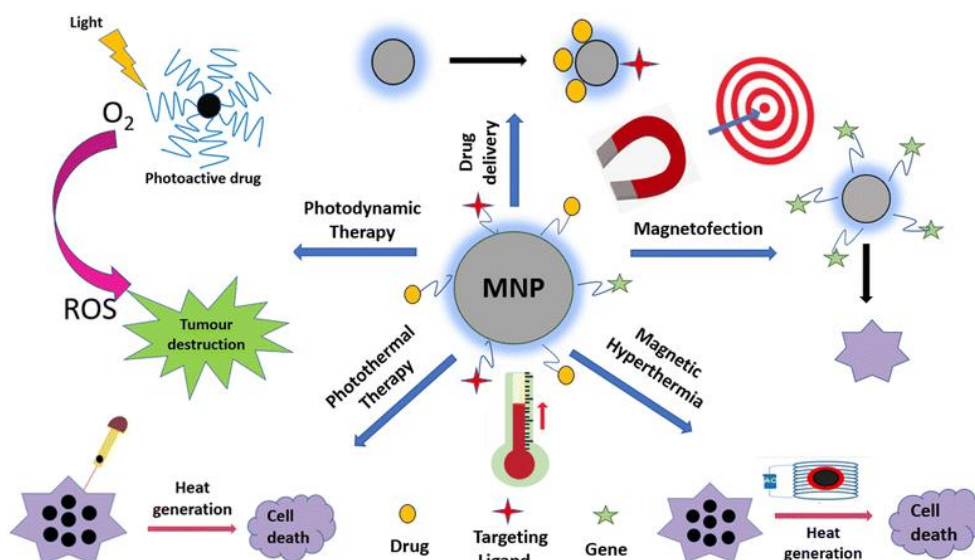
Figure 3: Various different uses for MNPs in biomedical applications[ix].

1.3 Super Paramagnetic Iron Oxide Nanoparticles (SPIONs)

Among the other MNPs, iron oxide has been chosen for its superior saturation magnetization, its facile and abundant nature, its exceptional biocompatibility, and a plethora of surface functionalization capabilities[x]. Super Paramagnetic Iron Oxide Nanoparticles (SPIONs) have found many uses, especially as an oncological diagnostic and treatment vehicle. It has found use in medical imaging through Magnetic Resonance Imaging compared to other Magnetic Nanoparticles. SPIONs boast a superior magnetization value increasing the effect of magnetic fields needed and reducing the amplitude of those fields to operate in the body.

Figure 4: SPION specific biomedical applications[xi].

1.4 Magnetism

Magnetic behavior arises from the orbital and spin angular momenta of electrons in material and their aggregate interactions. This is quantitatively described by the quantity, magnetization. This is defined as net magnetic dipole moment per unit volume of material. The proportionality of a magnetic response of a material is given by its magnetic susceptibility.

In the absence of long range magnetic momenta ordering, the materials can be put into two groups; dia and paramagnetic do not form long range magnetic orderings. In the case where long range magnetic momenta orderings are present, they are classified as ferro, ferri, and antiferromagnetic materials. Based on the susceptibility, materials can be divided into diamagnetic and paramagnetic materials.
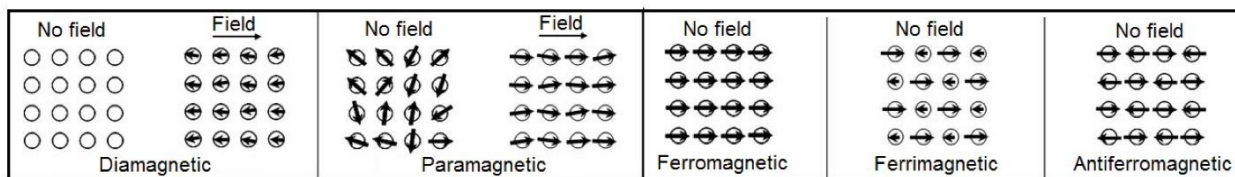
Figure 5: Diagram depicting the behavior of Diamagnetic, paramagnetic, ferromagnetic, ferrimagnetic, and antiferromagnetic materials respectively[xii].

Diamagnetic particles have a negative susceptibility, or will oppose an externally applied magnetic field. Meanwhile paramagnetic materials are the opposite and will align with an applied external magnetic field. This is a result of the conservation of momentum as diamagnetism occurs when the shells are filled resulting in net zero orbital and spin angular momentum. Paramagnetic materials have a net dipole moment per particle of material. These moments align randomly into domains, due to thermal effects resulting in a bulk net zero magnetic moment. These domains are also governed by energy exchanges within the system of particles:

1. The energy involved in aligning the magnetic moments

2. The magneto-crystalline structure energy that comes from the spin-orbit coupling

3. Magnetostatic energy

When an external field is applied, all of the domains align with the external magnetic field. Upon removal of the external field and sufficient time the paramagnetic materials reach net zero spin within newly formed domains. The temperature dependency is described by the Curie Weiss law, which states that the magnetic susceptibility of a

material below a specific temperature (The Curie Temperature) becomes

ferromagnetic[xiii]. Ferromagnetism is the phenomenon of spontaneous magnetization, or

magnetization that appears in the complete absence of applied magnetic fields. Below

this temperature materials tend to be antiferromagnetic and ferrimagnetic. Ferromagnets,

unlike their paramagnetic counterparts, do not relax to the same domains, making a non-

reversible change known as hysteresis. When characterizing this relationship of applied

field and saturation magnetization an M-H curve is used detailing the hysteresis.
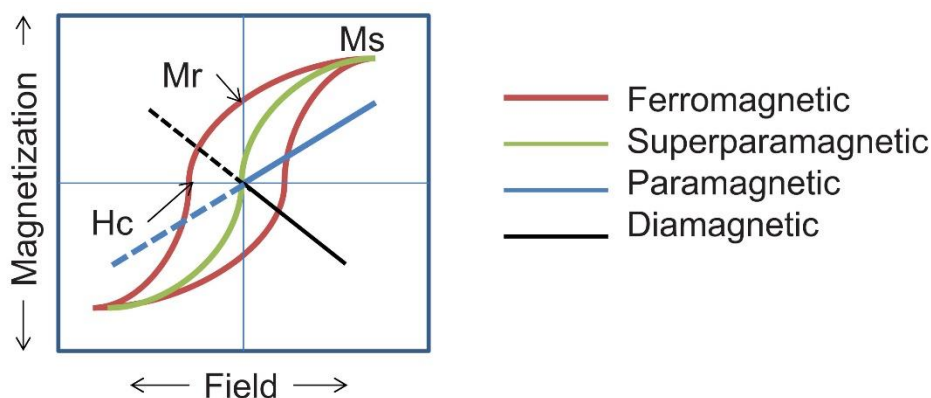
Figure 6: Hysteresis loops for the different magnetic behaviors[xiv].

Magnetic saturation refers to the state reached in a sample when increases in applied

external magnetic field H cannot increase the magnetization of the material further. At

saturation, the total magnetic flux density B does not increase with increases in applied

external fields, resulting in diminishing returns for magnetic energy applied. Saturation is

a characteristic of ferromagnetic and ferrimagnetic materials, such as iron, nickel, cobalt,

and their alloys. Saturation is most clearly seen in a hysteresis loop. As the H field

increases, the B field approaches a maximum value asymptotically, and from this the

saturation magnetization of the material is determined. This phenomenon arises from the non-linear permeability of free space for materials at large scales.

The magnetic properties of individual domains as they relate to a group of domains in the same bulk material is also given by a quantity known as anisotropy. Anisotropy refers to having a physical property that has a different value when measured in different directions. In the magnetic sense it refers to the magnetic energy required to change the direction of a magnetic dipole, measured from the energetically favorable direction (minimum), and increasing in required energy. The energetically favorable direction is along an axis called an "easy axis."

The three most important types of anisotropies are shape anisotropy, surface anisotropy, and magneto-crystalline anisotropy. As the size decreases, the surface anisotropy decreases and since the particles are spherical their shape anisotropy is minimized. Hence, the dominant anisotropy for spherical nanoparticles will be magneto-crystalline in nature.

With small enough particles the thermal energy is comparable to the anisotropy energy, or the energy required to flip along the energetically favorable axis. When this thermal energy is large compared to the anisotropic energy then the particle can freely flip along the energetically favorable axis. The relaxation time, the average time one of these jumps takes is given by the Neel-Brown relation:

$$\tau_n = \tau_0 * \exp\left(\frac{K * V}{k_B * T}\right)$$

Where τ_0 is a microscopic timescale for transitions, usually around $10^{-9} - 10^{-13}$ s, k_B is the Boltzmann's constant and T is temperature, K is the anisotropic energy density and V is the volume. As the temperature decreases, the relaxation time increases. From here we get the temperature at which this freedom occurs, known as the blocking temperature. This temperature is determined in the Zero-Field Cooling (ZFC) measurement. The magnetization changes in response to the temperature. The peak magnetization as a function of temperature gives the blocking temperature. Below this temperature the spins are essentially frozen in place, removing their ability to behave as paramagnets. Above this temperature the particles are able to flip freely enabling paramagnetic behavior, aligning with applied external magnetic fields.
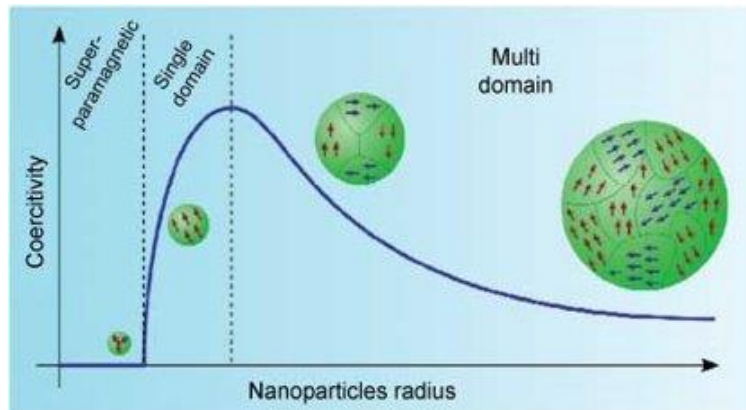
Figure 7: A diagram describing the coercivity required for the various particles size.

When the size of magnetic particles get below a critical value, the energy cost of domain wall formation is higher and subsequently unfavorable. Single domain particles become favorable. Within these single domains all of the spins are aligned, which is also known as possessing a super spin. These super spins yield a large magnetic moment for the

individual domain. Super-paramagnetism occurs when a super spin paramagnetic domain shows no hysteresis with a changing magnetic field. For Iron oxide this behavior is observed when it is in nanoparticle form.
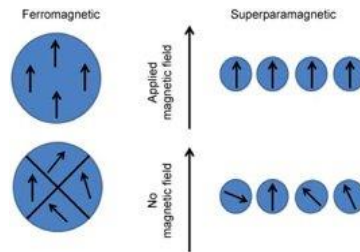
Figure 8: Comparison of Ferro magnetic behavior and super paramagnetic behavior.

In this study the model which will be used will be the Langevin function for describing the magnetization for a collection of non-interacting superparagmagnetic nanoparticles. This is usually indicated by an "S" shape on the M(H) curve taken by a magnetic characterization machine. The Langevin is denoted by:

$$M = M_0 * [Coth(\chi) - \frac{1}{(\chi)}]$$

And

$$\chi = \frac{M_s * V * H}{k_b * T}$$

Where M_0 is the saturation magnetization, M_s magnetic moment, H is the applied magnetic field, V is the volume, T is the temperature and k_B is Boltzmann's constant.

1.5 Magnetic Heating and Linear Response Theory

Applied magnetic heating can be understood via the Linear response theory, an

approximation method that describes the evolution away or toward equilibrium under

perturbative conditions[xv]. The work done on a magnetic system is converted into internal

energy for that system. The heat generation is primarily through the processes of Néel

and Brownian relaxations. During Néel relaxation the moments fluctuate under the

applied alternating Magnetic Field. This is interacting with the magnetic crystalline

energy barrier. Meanwhile, during Brownian relaxation the particles heat the suspension

due to drag between the particles and the liquid, when the particle rotates to align with

the applied field. Both of these occur in parallel so a combined relaxation effect is

observed.
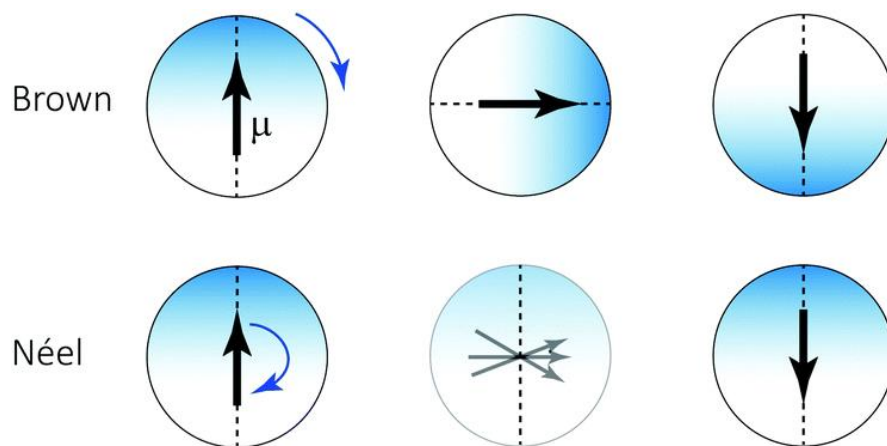
Figure 9: Brownian and Neel relaxations[xvi].

The Linear response theory in this scenario surmises that the energy applied by the

magnetic field to be proportional to the response of the system of magnetic particles.

$$P = \frac{\mu_0 * H_0^2 * \chi * \omega^2 * \tau}{2} * \frac{1}{1 + (\omega * \tau)^2}$$

In the low frequencies limit, where $\omega * t \ll 1$ the second portion approaches zero, then we get:

$$P = \mu_0 * H_0^2 * \chi * \frac{\omega^2 * \tau}{2}$$

Where P is the power dissipated, μ_0 is the permeability of free space, H_0^2 is the square of the amplitude of the oscillating magnetic field, χ is the magnetic susceptibility of the magnetic particles, ω is the frequency of the alternating magnetic field, and τ is the effective relaxation time, which is given by:

$$\frac{1}{\tau} = \frac{1}{\tau_N} + \frac{1}{\tau_B}$$

Where τ_N is the Néel relaxation time and τ_B is the Brownian relaxation time.

1.6 Hyperthermia

Hyperthermia, from Latin which means literally "above heat" refers to when heat regulating mechanisms of organisms fail. In the case of medical treatment, the goal is to cause these regulation mechanisms by inducing hyperthermia to fail in order to kill the offending organism. As a treatment hyperthermia falls into three categories: local, regional, and whole body. Whole body refers to treating the entire body through

something like hot wax or full body infrared radiation. Regional refers to a specific organ

or subsystem of the body, usually with ultrasound or radio electromagnetic radiation

(usually around 13.56 MHz[xvii]). Finally, local refers to heating a smaller area of interest,

in the case of this research, a tumor. Localized hyperthermia is quite difficult due to the

size involved and methods of heat transfer to smaller targets. However there are studies

that show that Magnetic Hypethermia (MHT) is superior to other hyperthermic

treatments, specifically hot water[xviii].

Cancer cells are not able to tolerate heat as well as healthy cells due to reduced blood

flow and increased oxidative stress due to being acidic. Many studies[xix] have found that

increasing the local temperature to 42 to 46 degrees Celsius induces localized

hyperthermia, causing damage and subsequent death of cancer cells. Within this

threshold, healthy cells are able to dissipate the heat and avoid detrimental effects.

Utilizing the lower viability cancer cells have after exposure to high temperatures, an

alternating magnetic field is applied to the nanoparticles in order to create localized heat

to the area of interest/infection known as local Magnetic Hyperthermia (MHT).
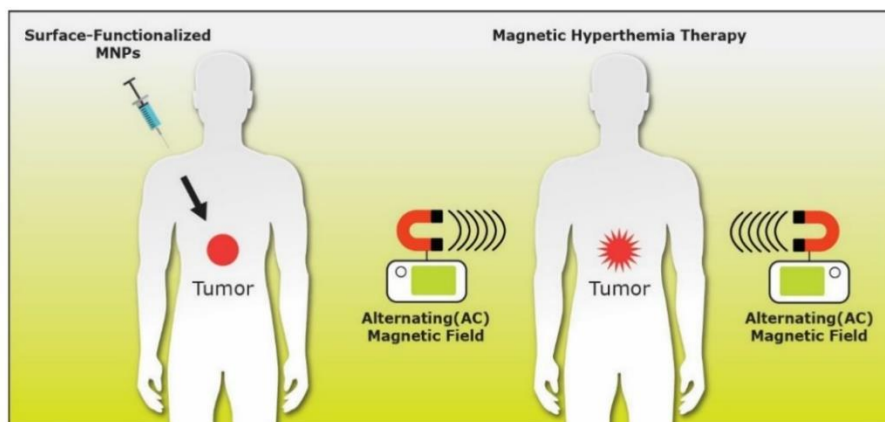
Figure 10: A diagram depicting how functionalized MNPs are used in MHT[xx].

The cell viability drops rather quickly after exposure, while allowing the non-cancerous cells to survive. Additionally, some studies have found that MHT can kill tumors at distant sites including metastatic cancer cells[xxi].

1.7 Photothermal Therapy (PHT) and Photon Plasmon resonance
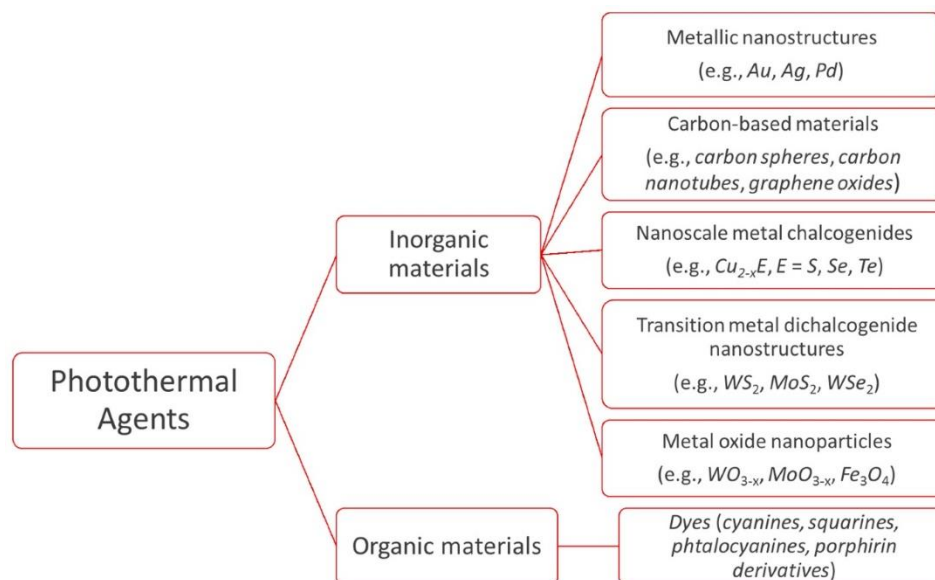
Figure 11: Like nanoparticles, there is a large array of photothermal agents as well. The present study will focus on metallic nanostructures and metal oxide nanoparticles[xxii].

According to the literature, there are different organic and inorganic materials that are being investigated as potential photothermal agents, as shown in Figure 11. This study will focus specifically on metallic nanoparticles for decorating SPIONs. In metals, photothermal effects arise from the property known as surface plasmon resonance. When metals are formed from the individual atoms the electrons become delocalized over the surface of that metal. These electrons are known collectively as Surface Plasmon. The term plasmon refers to a quantum or a quasiparticle connected to a local collective oscillation of a charge density. In this case the surface plasmon is referring to the free electrons in the conductive band of our metals. The energy levels for electrons in atoms are discrete as has been established[xxiii][OBJ]. However, in metals, as the number of atoms are increased, the number of viable energy levels also increases. In bulk metal this effectively gives a continuous energy range.

With nanoparticles this range becomes quasi-continuous. In bulk metal the surface plasmon resonates in phase with incoming light. This oscillation is scattered back into the incident medium. Due to their semi-discrete or quasi-continuous nature, nanoparticles cannot resonate with all wavelengths of light. As the wavelengths change there is a particular frequency that causes no-net oscillation due to destructive interference on the surface plasmon. This energy is converted into heat through relaxing a photo-excited electron. This heat is then dissipated through phonon-phonon coupling after the relaxation period.
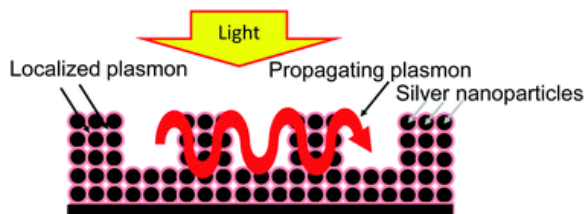
Figure 12: Diagram depicting the interaction of incoming light with the localized plasmon, usually conduction band electrons, causing a resonance on the surface of the particle[xxiv].
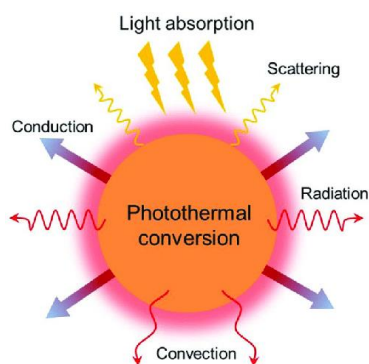
Figure 13: Depiction of the photo thermal conversion process due to plasmonic resonance[xxv].

The physical characteristics of the particle also affect the photothermal effect, specifically the peak frequency that generates the maximum heat. Most notably, the shape and size, which will affect the wavelengths and amplitudes that the surface plasmon will have a resonance response. Silver[xxvi][xxvii] is a prime choice since there exists a large number of studies on the photothermal characteristics it possesses. One of the reasons it has been studied so much in medicine is because silver also has the ability to bind to and destabilize DNA of target cells. Silver in general has seen a wide variety of biomedical applications in cancer therapy as Figure 14 shows. In the case of treating cancer, preventing their reproduction is a superior trait when dealing with metastasizization.
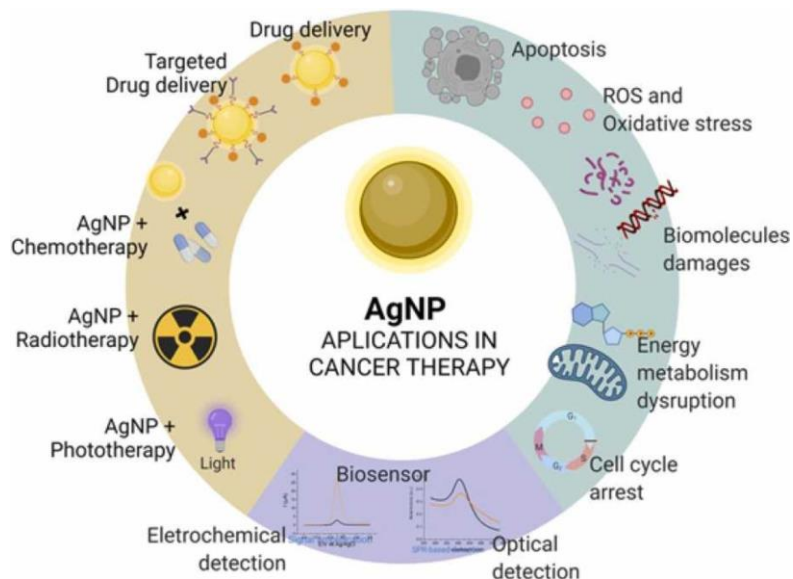
Figure 14: The various uses of silver in cancer therapy has a similar number of complimentary applications to that of SPIONs[xxviii].

The combination of this platform with SPIONs allows them to be placed and injected near and into cancerous cells in addition to generating localized hyperthermia. Additionally, several studies have found SPIONs to have a photo-induced plasmonic resonance response in a range that overlaps with that of silver for incoming light[xxix].

1.8 Specific Absorption Rate (SAR)

The heating efficiency of the SPIONs during MHT in this study are given by Specific Absorption Rate (SAR). This is defined as the thermal power per unit mass of magnetic material generated while in an alternating magnetic field. For ferrofluids it depends upon the fluid characteristics, the applied magnetic field properties, and the properties of the SPIONs, such as shape, size, distribution, and concentration[xxx]. The ideal fluid is limited to biocompatible fluids, in this case water-based is ideal. Additionally, there are limitations on how the alternating magnetic field can be used on the human body.

The upper limit of the product of the amplitude and the frequency of the AC magnetic field that can be used in clinical trials without generating eddy currents and nerve stimulation is 5 *10^9 A*m^{-1}s^{-1} [xxxi]. Finally, there is a requirement to have the SPIONs be biocompatible and have superparamagnetic properties at physiological temperatures. This is to avoid toxic effects of SPION aggregation and toxic immune response.

The heating efficiency of the materials will be given by the SAR[xxxii], which is determined by the rate of change in heat per unit of material. First, the heat flow rate is determined by:

$$\frac{dQ}{dt} = m * c * \frac{dT}{dt}$$

Where Q is the heat in Joules, m is the mass of the sample, c is the specific heat of the suspension, T is the temperature, and t is the time. From here we calculate the SAR as:

$$(SAR) = \frac{\frac{dQ}{dt}}{m_{Fe3O4}}$$

1.9 Scope of this thesis

Objectives, Significance, and Justification

This methodology of localized hyperthermia is very useful when compared to other methodologies of oncological treatment, which essentially bombard the body with radiation or drugs to kill cells that develop quickly. There is often a lot of collateral

damage or undesired side effects resulting in secondary and tertiary ailments to the patient which complicate recovery and reduce quality and length of life.

Additionally, reducing the amount of resources that the body needs to use to repair itself improves health outcomes. Reducing the number of other treatments for these undesired effects benefits the patient and the medial system as a whole.

With current methods of functionalization there is a limit to how much heat generation potential there is for SPIONs using only MHT. There is a limit to how the concentration of the SPIONs are acceptable to prevent toxic effects[xxxiii]. There is also a limit to the amplitude and frequency of the alternating magnetic field. The main obstacle to the current usage of SPIONs is that when debris and cellular structures interact with the SPION, it increases the moment of inertia for the particle, reducing the amount of rotation, and by extension, the amount of heat produced by the alternating magnetic field.

There are several methods to overcome this reduction in heat generation. One is the shape[xxxiv] of the particles, as this affects the ability to rotate by altering the shape anisotropy. This is affected by the functionalization process. There are many factors that can go into the differing shapes and their uses but this requires a great deal of study for fine tuning. Generally, spherical functionalization has been regarded as the most utilitarian shape. The second method to overcome the reduction in heat generation is altering the magnetic saturation of the SPION composition[xxxv]. Adding other magnetic metals has a pronounced effect on the magnetic saturation of the composition but is often not facile to manufacture and requires tuning to avoid cytotoxicity[xxxvi]. A third method is

a mixture of these two methodologies to blend their properties. This has seen some success but is not facile[xxxvii].

An alternative method, which will be the primary focus of this study, was introducing photothermal agents into the SPION composition. This represents a very facile and effective method for improving the thermal output of the SPION composition. In particular, silver atoms added to the SPION composition will be the focus of this research. If the total heat generated from the alternating magnetic field of the compound comprised of both SPIONs and Silver atoms is comparable to a pure SPION compound, then this methodology would lead to new avenues of research for SPION based oncological treatments. There has been promising research carried out regarding the use of MHT and PHT simultaneously on SPIONs to help them overcome the barriers to successful treatment presented in either case alone[xxxviii].

The scope of this thesis will be in three parts: first, to explore the effect on magnetic response when decorating SPIONs with silver NPs; second, to compare the relative SAR values for MHT, PHT, and combined heating; third, to compare green synthesis and conventional synthesis of the SPIONs and Ferrofluids for their heating performances.

Chapter 2: Synthesis and Characterization Methods of Magnetic Nanoparticles

2.1 SPION Synthesis methods

When generating SPIONs and AgNPs there are many methods that have been utilized.

Physical methods include: Gas-Phase deposition, electron beam lithography, power ball

milling and combustion. While Chemical methods include: co-precipitation, thermal

decomposition, microemulsions, and hydrothermal. Finally there are biological methods

which utilize bacteria, fungi, and microorganisms[xxxix]. For many of the synthesis methods

there are issues with consistency in size, functionalization, and being biocompatible

during functionalization. Most studies use a host of chemicals during the synthesis

process, many of which require specialized lab conditions and the ability to store and

dispose of toxic chemicals. Additionally, for the physical methods there is a great deal of

specialized equipment needed for those processes as well. Co-precipitation and

hydrothermal provide monodispersed, facile, and biocompatible methods of synthesizing

nanoparticles. During co-precipitation iron precursors are reduced to iron oxides by a

weak reducing agent, conventionally sodium hydroxide, ammonia, and the like. The

reaction equation is:

$$Fe^{2+} + 2\ Fe^{3+} + 8\ OH \rightarrow Fe_3O_4 + 4\ H_2O$$
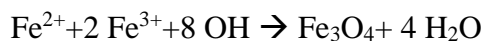
Meanwhile during hydrothermal crystal growth of minerals is encouraged using high

temperature and pressure, usually below 300°C and organic solvent. This study will use

coprecipitation for the generation of SPIONs and hydrothermal for silver decoration.
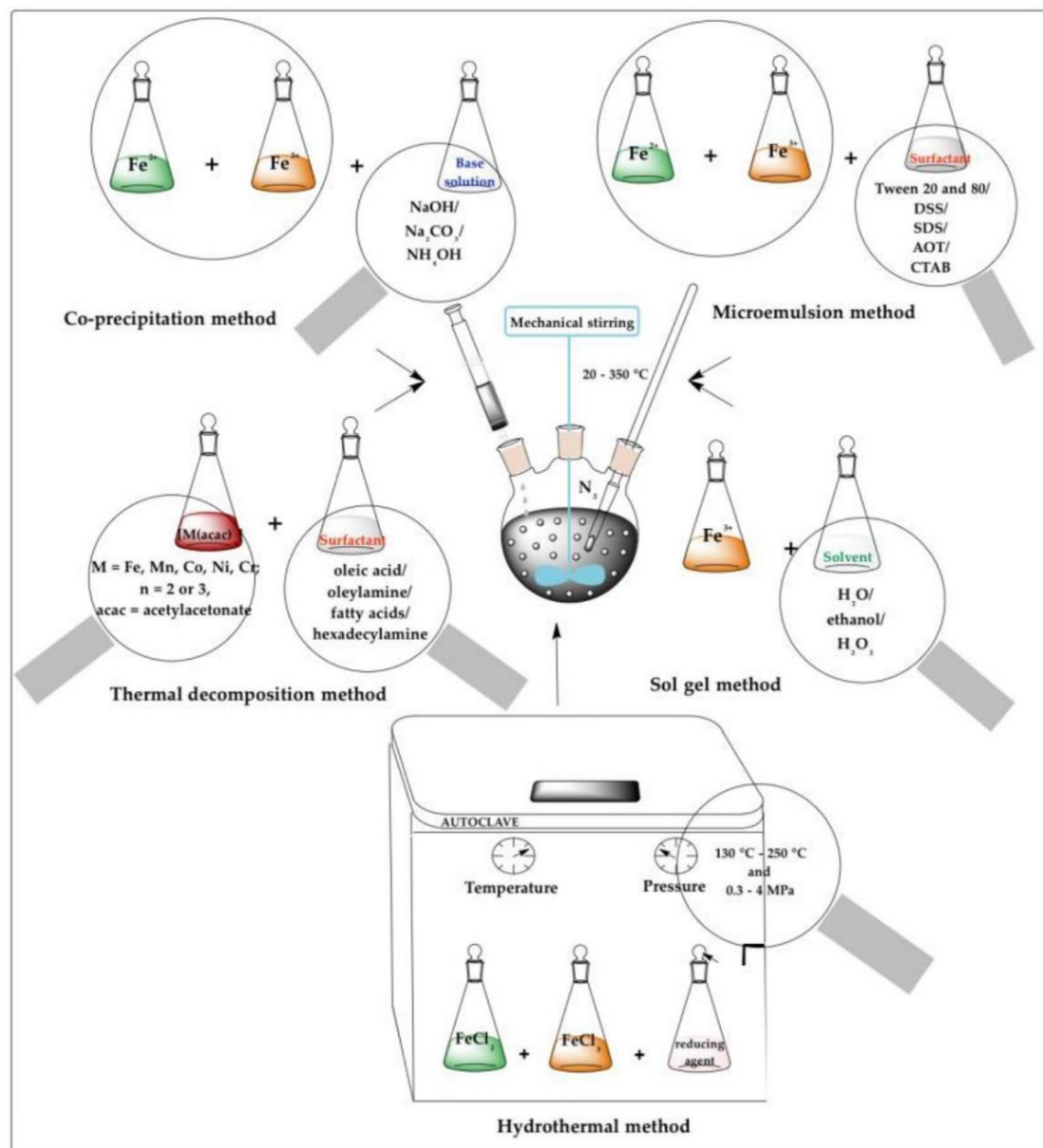
Figure 15: the various chemical methods of SPION synthesis. This study will focus on co-precipitation without inert

gas[xl].

2.2 Green Synthesis

This study will also explore the rising trend of green synthesis methods. With the

observable impacts on the environment due to human activity growing at exponential

rates, methods that reduce the amount of environmental impacts are becoming more and more desirable. Balancing the environmental impact with efficacy is at the front of this effort. There are many promising avenues and the present study has gone the path of utilizing Green Synthesis[xli] processes for generating the nanoparticles. This also has the added benefit in the medicinal usage to being bio-compatible. Green synthesis utilizes plant extracts or bio-polymers for capping and stabilizing. Egg White (EW) show promise to be among the best for its environmental, economic, and physiological impacts. For the mono-colloidal suspension citric acid(CA) and water is used, in lieu of dextran[xlii]. Honey will be used as a Hydrothermal reducing agent for the silver decoration of the SPIONs[xliii].

The significance of this research is in further improving upon nanotechnology for a growing area of concern for medical applications as well as exploring ways to minimize human impact on the environment while pursuing new technologies. The justification is tied to improving quality of life for both humans and the environment amidst increasing health problems due to cancer and an increasingly unstable environment due to human activity.

2.3 Surface modification/Functionalization

For particles in the nano particle range the surface energy is rather high. This arises from having a larger surface to volume ratio[xliv]. Additionally, MNPs often have hydrophobic characteristics on their surfaces. Due to this the particles tend to aggregate. In most biomedical applications aggregation is not desired and results in clots or other harmful

effects. This aggregation also leads to more chemical activity and generally depresses the magnetic characteristics of the material. To alleviate the aggregation and improve the stability of the nanoparticles, they are coated with a surfactant and suspended in a mono-colloidal suspension. The two methods employed are steric and electrostatic repulsion. Steric is often difficult to predict and make uniform while electrostatic is relatively easy to understand given the ionic strength and pH of the solution during and after synthesis[xlv].
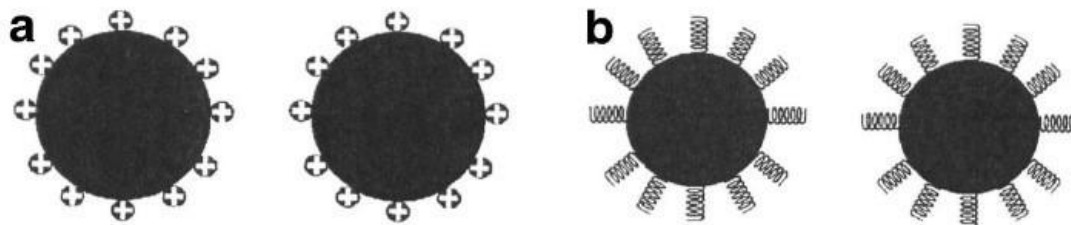
Figure 16: (a) depicts electrostatic repulsion during surface modification, while (b) depicts steric repulsion from surface modification[xlvi].

The several most common surfactants that are used are Dextran, PEG, and citric acid. The choice is often a result of the application. For instance, Dextran is highly biocompatible, while PEG has the longest circulation time. For this study, citric acid has been used. This is due to its large capacity to be further functionalized and in keeping with the green synthesis methodology.
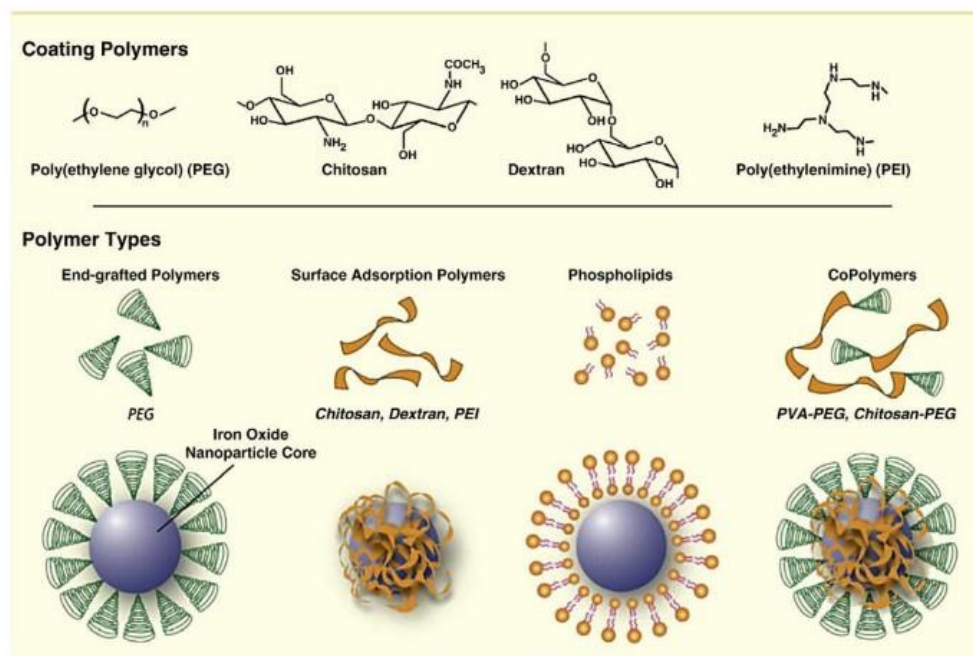
Figure 17: Examples of different coating polymers for steric repulsion[xlvii].

Characterization techniques

2.4 X-Ray Diffraction (XRD)

Electromagnetic radiation with wavelengths between 0.1 to 10nms with energies from 100 eV to 100keV are known as X-rays. In determining the arrangement of atoms and molecules within crystalline materials XRD is able to identify the materials present. These rays interact with the different layers of atoms to diffract, when constructively interfering, producing sharp maxima. The angles at which this occurs depends on the crystalline structure of the material. The angle formed is between the incident ray and the atomic planes.
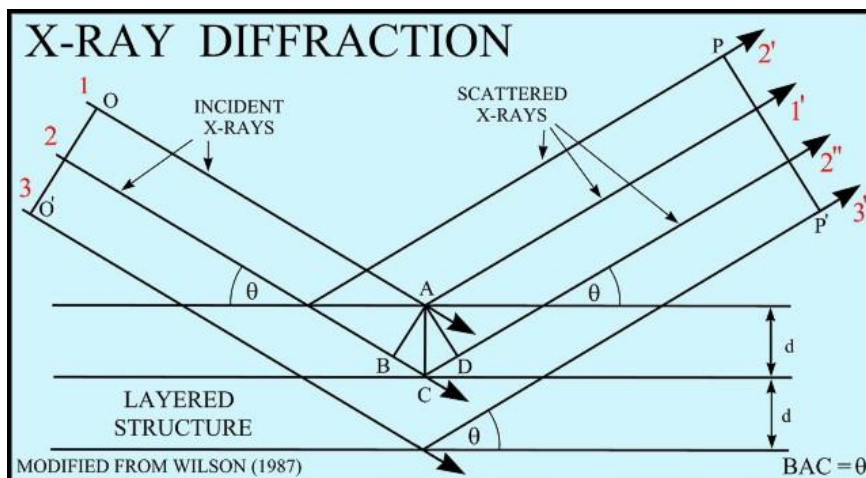
Figure 18: Depiction of XRD[xlviii].

From here the Debye-Scherrer equation Is used to determine the average crystalline size

of the particles:

$$d_{avg} = \frac{k\lambda}{\beta_{FWHM} \cos \theta}$$

Where λ is the wavelength of the incident x-ray, *k* is the shape factor(0.94 for spherical

particles), β*FWHM* is the fullwidth half maxima measured from the unprocessed data and in

radians.

2.5 Tunneling Electron Microscope (TEM)

To determine the shape and confirm the size of the SPIONs and Ag-SPIONs a Tunneling

Electron Microscope (TEM) was utilized. During operation, a high voltage electron beam

passes through the sample. The sample, originally in powder form, is suspended in an

acetone solution. The electrons either scatter, or tunnel through hitting a fluorescent

screen. The gradations found on the fluorescent screen give a relief based on how thick the material is, giving an image. This solution was placed into a vacuum inside the TEM apparatus. From this the size distribution and shapes will be confirmed. To determine the size distribution the log normal fitting equation below will be used:

$$f(D) = \frac{1}{\sqrt{2\pi}\sigma D} \exp\left\{-\frac{[ln\frac{D}{D_o}]^2}{2\sigma^2}\right\}$$

Where D is the diameter, D_o is the probable diameter, and σ is the size distribution[xlix].
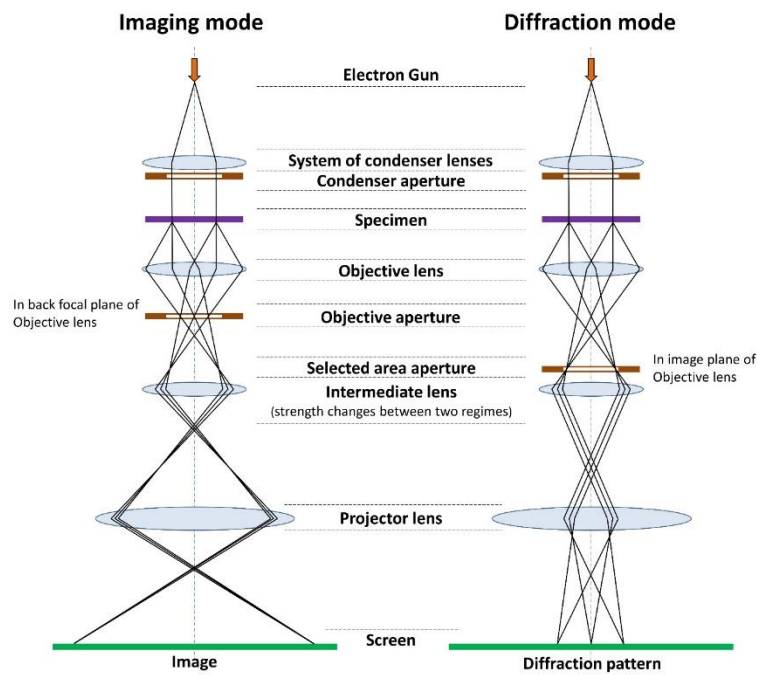
Figure 19: Schematic of TEM operation. This study utilizes the imaging mode.

2.6 Vibrating Sample Magnetometer (VSM)

A Vibrating Sample Magnetometer utilizes Faraday's law of induction to measure the

magnetic properties of a sample placed into the sample holder. The holder allows for the

sample to vibrate and is on an arm that moves the sample through a magnetic field that is

sensed and recorded by electromagnets via their induced coil. The resulting current gives

data about the strength of the magnetic field of the sample[l]. The setup is described in the

following figures.
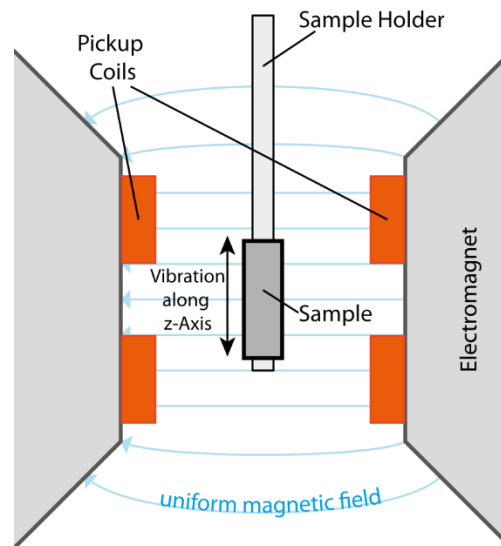
Figure 20: Schematic of VSM as the sample is moved and vibrated inside the uniform magnetic field[li].
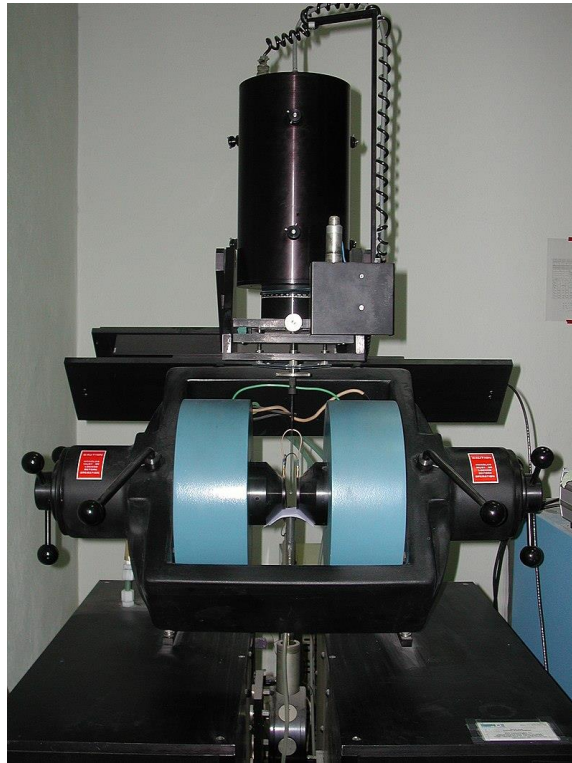
Figure 21: External view of a VSM[lii].

The information from this will generate an M(H) curve to which the Langevin model will be applied.

2.7 Magnetic Hyperthermia

The SPIONs and Ag-SPIONs are made into a ferrofluid. From here an alternating magnetic field is applied. This generates a change in temperature as the particles relax. The rate at which this heating occurs will determine the efficacy of the combined platform. An Ambrell Easy heat station will be run an appropriate frequency until the temperature of the fluids reach a range between 50-60° C. The temperature was measured from the center of the container holding the ferrofluid. An alternating magnetic field is applied to a solenoid producing an alternating magnetic field. To dissipate the heat in the

circuit there is a water pump attached. During this measurement the fluid is placed inside of the solenoid and a fiberoptic cable is used to record the temperature from inside the center of the tube containing the ferrofluid. This is run to a program titled Opticon. From here the temperature and the time is recorded.

Figure 22: MHT set up, with optical fiber thermometer, tube, and current carrying coil.
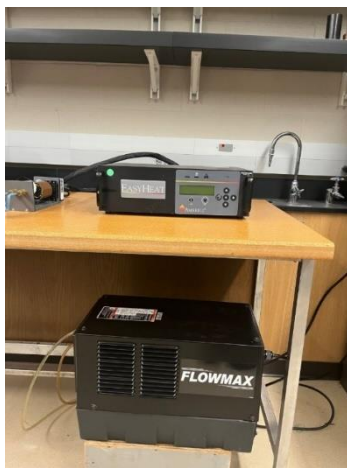
Figure 23: Ambrell easy heat station and water coolant system. This is to prevent the coil from overheating.

Figure 24: Complete MHT data taking station.

2.8 Photothermal Heating

A laser diode is used to provide to provide light of the correct wavelength and power, a

commercial laser[liii] ,typically used for engraving, was used, with wavelength 808 nm and

a maximum output power of 1.2 W. LASER or Light Amplification by Stimulated

Radiation [liv] , electrons are excited in a gain medium. As the electrons in the material

relax from their excited state monochromatic light is emitted to obey conservation of

energy. See figures 10 and 11 for a visual. This quantum mechanical effect has been used

following Einstein's prediction of on the nature of discrete energy levels and their

transitions. The first laser was a modified maser (Microwave Amplification by

Stimulated Radiation), and focusing in the optical range. The first patent for the Laser

was in 1957 by a Japanese engineer. The laser was turned on, shining onto the surface of

the ferrofluid. The temperature was measured from the center of the tube, in the same

fashion as the MHT.

Figure 25: Configuration for both PHT and combined heating measurements. The alternating magnetic field is turned off while the laser, pictured above the coil, shines upon the ferrofluid.

Chapter 3: Experimental

3.1 Conventional Superparamagnetic Iron Oxide(SPION) Synthesis

Ferrous Chloride Lot 128205 and Ferric Chloride lot 931865 from Fisher Scientific were used

without further purification. Conventional SPIONs were synthesized with 3.014 g of ferrous

Chloride was dissolved into 5ml of 2M HCL. 8.105g of ferric iron chloride was dissolved into

20mL of 2M HCL. These were combined into a beaker and then stirred magnetically at 700 rpm

using a Fisher Scientific Isotemp magnetic stirrer. NaOH, at a molarity of 3M, was added drop

wise into the stirring solution until a pH of 11 was reached. The solution was stirred for 90

minutes. The resulting particles were then aggregated using a .1T magnet, washed, and dried.
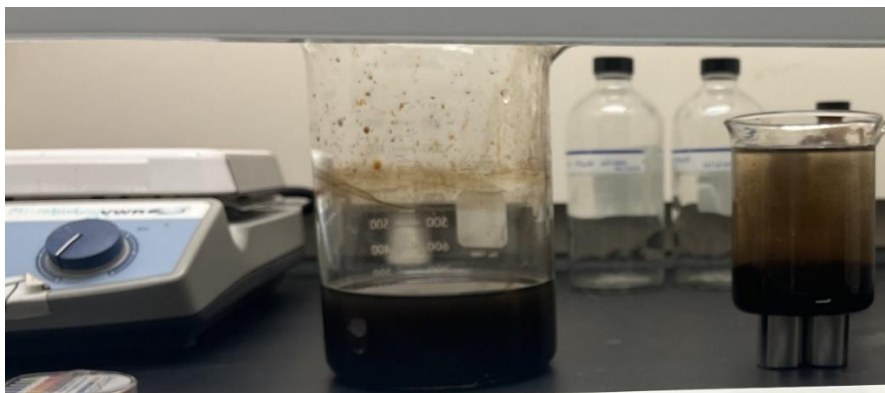
Figure 26: Washing and separation of SPIONs.

o   *Green Synthesis*

3.2 Green Egg white Superparamagnetic Iron Oxide (EW SPION) Synthesis

3.003 grams of ferrous chloride and 8.114 grams of ferric chloride from the before mentioned

sources, were separately dissolved in two separate beakers with 90 mL of deionized(DI) water,

under magnetic stirring for a few minutes each. An egg white(EW) aqueous solution was

prepared by adding 0.775g of EW dissolved into 20mL DI water. The EW is used as a capping

agent in lieu of Hydrochloric acid, which is usually used. All three solutions were then combined

and stirred at 700 rpm. NaOH at 3M was added dropwise until a pH of 11 was reached, then

temperature was set to 65°C and the solution was stirred for 90 minutes. After, using a magnet to

aggregate the MNPs, they were rinsed in DI water until a neutral pH was reached. The slurries

were then set out to dry. In this procedure EW was used as a capping agent. This is in contrast to

Hydrochloric Acid being used in the non-green synthesis process.
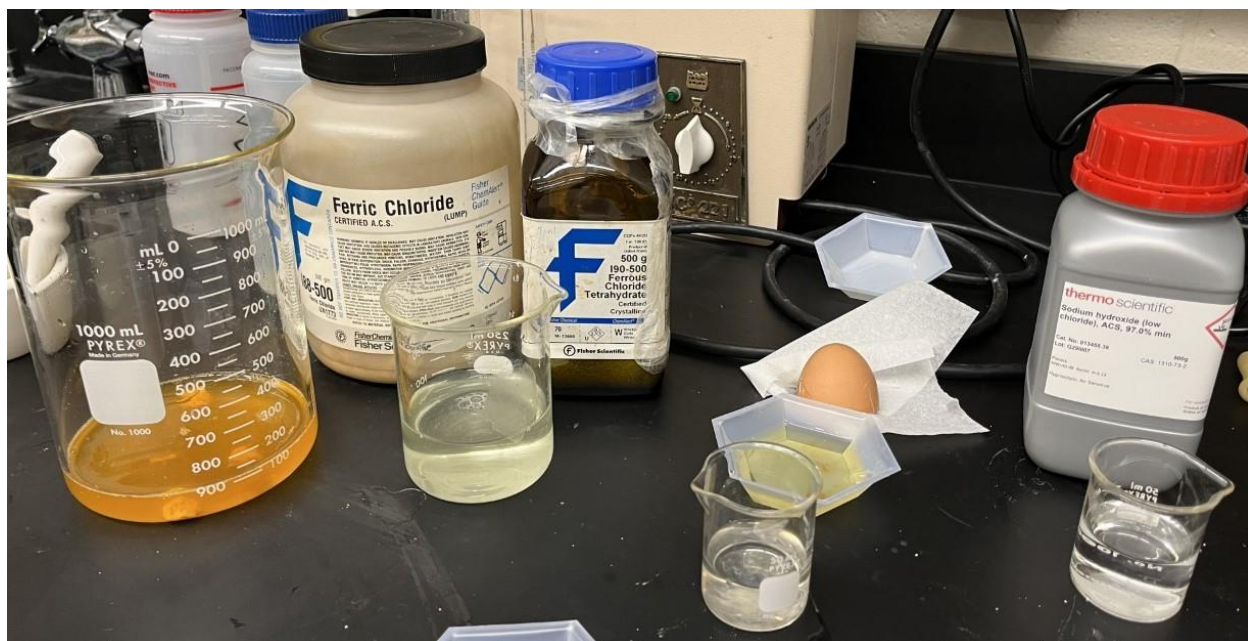
Figure 27: Precursors to green synthesis in solution form.

3.3 Silver Decoration of SPIONs and EW SPIONs

3.3.1 SPION silver decoration (Ag-SPION)

22 mg of Silver Nitrate, 1.013 g of commercial food-grade honey and 70mL of DI water were stirred for 15 minutes. 305mg of SPIONs were added and sonicated for ten minutes. The solution was then put into a Teflon lined autoclave and heated to 200°C for 75 minutes using a Blue oven, model BF51848A. They were magnetically collected upon cooling and left to dry. This was repeated twice.

3.3.2 EW SPION silver decoration (EW Ag-SPION)

18 mg of Silver Nitrate, 1.060 g of commercial food-grade honey and 70 mL of DI water were stirred for 15 minutes. 299 mg of EW SPIONs were added and sonicated for ten minutes. The

solution was then put into a Teflon lined autoclave and heated to 200°C for 75 minutes. They

were magnetically collected upon cooling and left to dry. This was repeated twice.

Figure 28: Oven used for hydrothermal silver decoration, Blue model BF51848A.

Creation of Ferrofluid

3.4 Ferrofluid preparation

A water based ferrofluid was prepared and synthesized using citric acid. 0.5g of SPIONs

were suspended into 50mL of DI water using a Bransonic 221 sonicator. A buffer

solution was prepared to bring the pH to 5.2 with SPIONs, citric acid, and NaOH. This

was heated to 80° C and stirred at 700 rpm. After 90 minutes the solution was cooled and

brought to a pH of 10.7. this produced a stable ferrofluid. This was done for SPIONs, Ag-

SPIONs, EW SPIONs, and EW Ag-SPIONs.

3.5 Characterization/measurements
3.5.1 XRD

All four samples were prepared in a powder form. A Rigaku Ultima-4 X-Ray Diffractometer 1.5 A Å radiation. A Θ-2Θ scanning mode with 20°-80° range, operating at a voltage of 40kV and current of 150mA was used to take the XRD spectrum for identification of the crystalline structure of iron oxide and silver. Crystalline size was also determine.

3.5.2 TEM
All four samples were prepared into a solution from powedered form. This suspension was loaded into a Thermo Fisher Talos F200X G TEM machine, with a beam current around 11nA for CTEM and 0.5 nA for STEM.

3.5.3 VSM

For all four samples the field dependence and temperature dependence of magnetization were measured using a Quantum design VersaLab magnetometer.

3.5.4 Heating Measurements

Three sets of heating measurements were taken, MHT, PHT, and Combined. This was done for SPIONs, Ag-SPIONs, EW SPIONs, and EW Ag-SPIONs. For MHT, an Ambrell easy heat station was used to generate an alternating magnetic field of amplitude 240 Oe (19.1 kA/m) at a frequency of 375 kHz. A sample of the ferrofluid was placed inside the current carrying coil. An Optocon fiberoptic thermometer was used to record the temperature of the sample in the center every ten seconds, until 55-60°C was reached.

For PHT, a commercial laser pointer was set to 600 mW and trained on the surface of the ferrofluid. An optocon fiberoptic thermometer was used to record the temperature of the sample, again at the center of the sample tube, until rate of change in temperature reached zero or the sampled reached 49-55°C.

Then the heating sources were combined. The samples were placed into the current carrying coil and had the laser trained on them. The Fiberoptic thermometer measured from the center. This was done until the temperature reached 55-60° or the rate of change in temperature was approaching zero.

Figure 29: Combined MHT and PHT heating configuration, with laser turned on.

Chapter 4 Results and Discussion

4.1 XRD Results
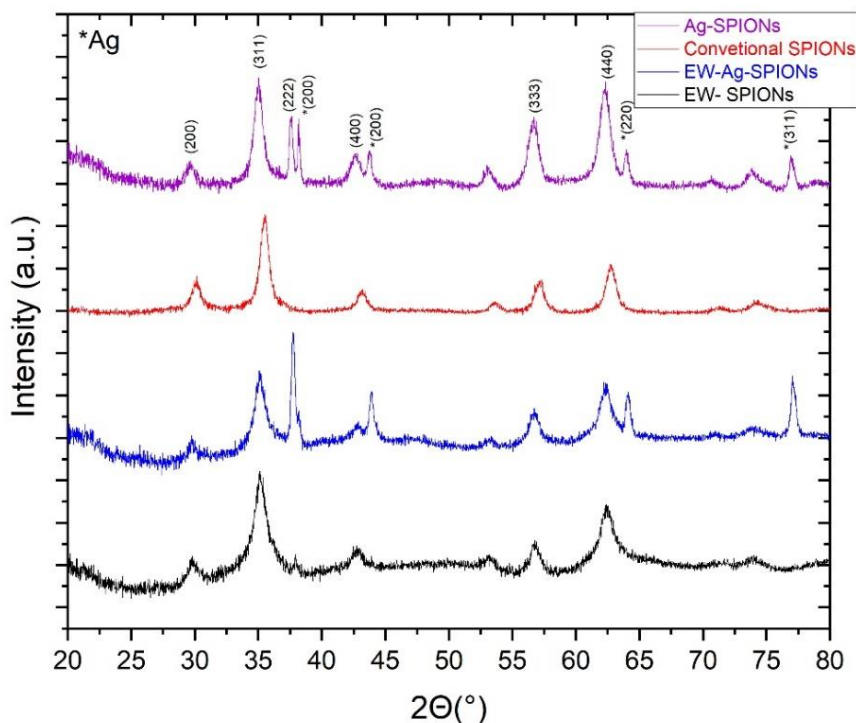
Figure 30: XRD Spectra for all four samples. Iron oxide and silver are present in the appropriate samples.

XRD Spectra from the SPIONS, Ag-SPIONs, EW SPIONs, and EW Ag-SPIONs were taken and analyzed. The peaks confirm that Fe_3O_4 was present according to the literature in the correct phase. For the composite peaks matching those of silver were found as well. The crystalline sizes were found to be 9.7 ± 0.1 nm for Fe_3O_4 and 31 ± 9 nm for Ag in the Ag-SPION sample, 10.8 ± 0.7 nm for Fe_3O_4 in the SPION sample, 8.0 ± 0.4 nm for Fe_3O_4 in the EW SPION sample, 9.6 ± 0.8 nm for Fe_3O_4 and Ag having a size of 23 ± 3 nm in the EW-Ag-SPION sample.

4.2 TEM
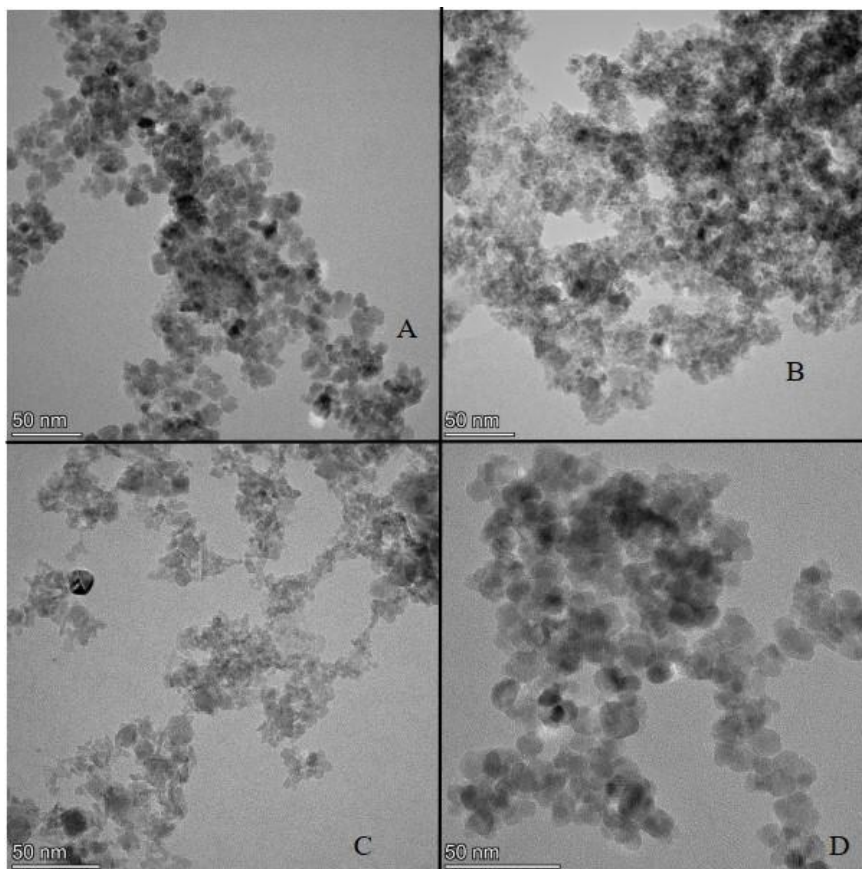
Figure 31:TEM images for A-SPIONs, B-EW SPIONs, C-EW Ag-SPIONs, D-Ag-SPIONs

Nanospheres were confirmed present in the prepared samples along with some agglomeration. The average diameters for the samples were estimated to be 11 ± 2 nm for Ag-SPIONs, 10 ± 3 nm for SPIONs, 7 ± 2 nm for EW SPIONs, and 10 ± 2 nm for EW Ag-SPIONs. The presence of silver was confirmed in TEM images as well, as shown in the figure below:
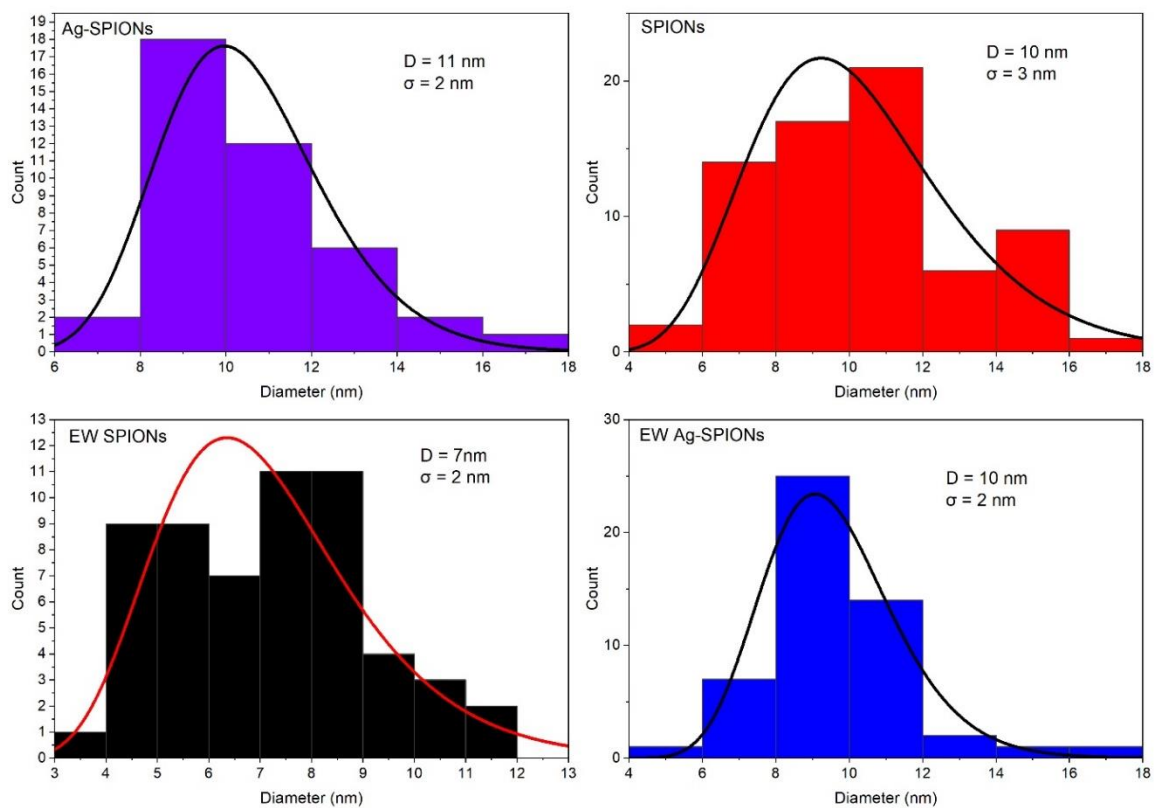
Figure 32: Log Normal Fit for all four samples.
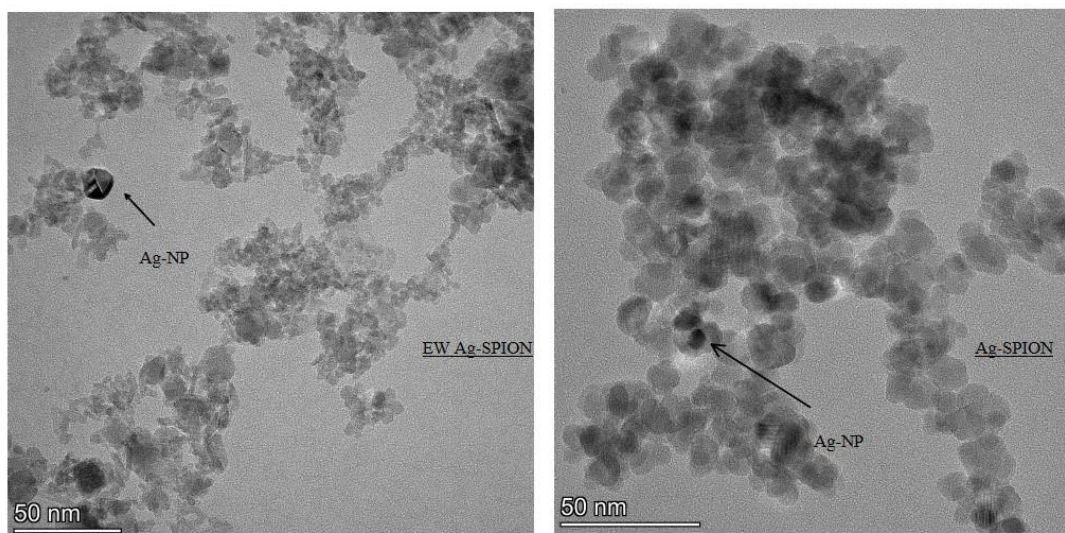
Figure 33: Silver decoration in EW Ag-SPION and Ag-SPION samples.

4.3 VSM Measurements
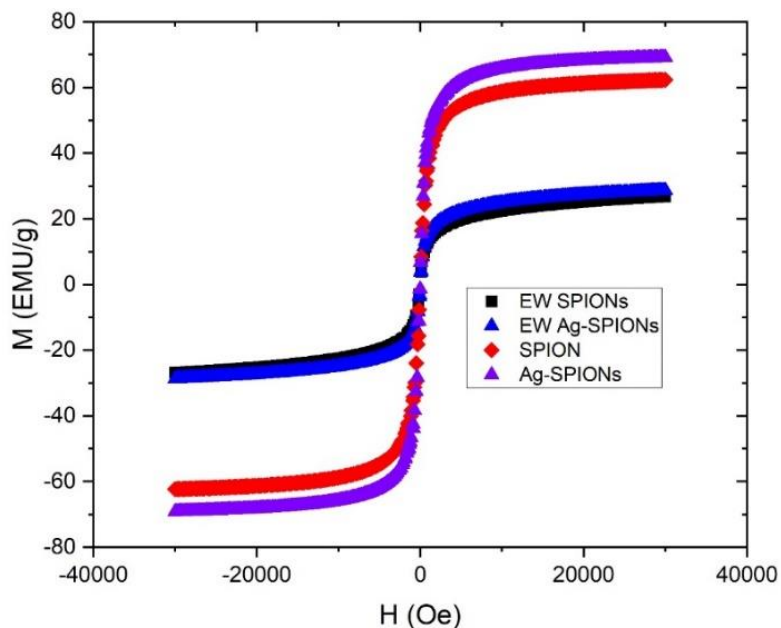
Figure 34: M(H) curve for the four samples. They display superparamagnetic behavior. The saturation magnetization was found to be about half for the samples with egg white as the capping agent.

M(H) curve for the four samples. They display superparamagnetic behavior. The saturation magnetization was found to be about half for the samples with egg white as the capping agent.

M(H) curve for the four synthesis methods. They were all found to display superparamagnetic behavior with no hysteresis at 300K.

A fit was done of the magnetization as a function of the inverse of the magnetic field applied to find the appropriate value of b. This expression was used from the relevant methods found in the literature[lv]:

$$\mathbf{M} = M_s(1 - \frac{b}{H^2})$$

Where M is the magnetization, M_s is the saturation magnetization, and H is the applied magnetic field.
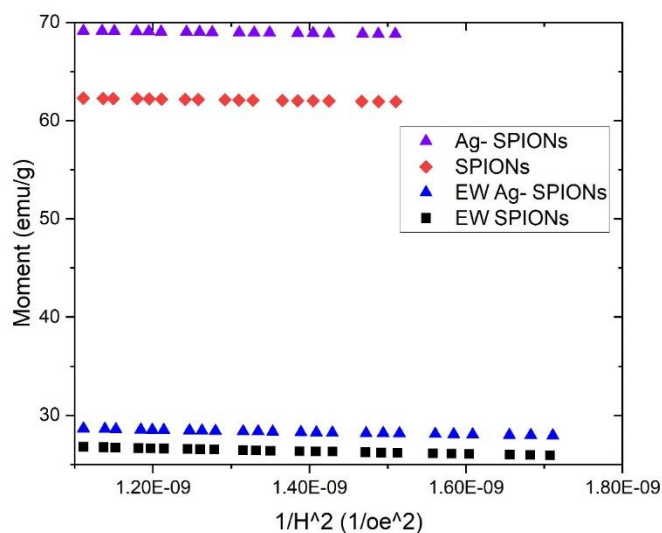
Figure 35: Magnetic moment as a function of the inverse of the magnetic field applied. This was used to calculate the effective anisotropy.

From the intercept of this fit the following saturation magnetization values were obtained, which are in agreement with the saturation values obtained directly from the M(H) curves.

Table 1: Saturation magnetization of the four samples. The uncertainty from the fit was 3 orders of magnitude smaller and were treated as negligible.

Sample	Saturation Magnetization (emu/g)
Ag-SPIONs	*70.0*
SPIONs	*63.3*

EW SPIONs	*28.4*
EW Ag-SPIONs	*29.9*

The b values were estimated to be $8.11 \pm 0.05 * 10^8$ oe^2 for Ag-SPIONs, $8.87 \pm 0.06 * 10^8$ oe^2 for SPIONs, $1.44 \pm 0.02 * 10^9$ oe^2 for EW SPIONs, and $1.15 \pm 0.01 * 10^8$ oe^2 for EW Ag-SPIONs.

The effective anisotropies, K_{eff}, were given by the following expression using a method from the literature[lvi]:

$$K_{eff} = M_s * \sqrt{\frac{15 * b}{4}}$$

Where M_s is the saturation magnetization and b is a constant related with the magnetocrystalline energy. From here the calculated effective anisotropies were found to be 41 ± 2 K J/m^3 for Ag-SPIONs, 41 ± 2 K J/m^3 for SPIONs, $32.3 \pm .8$ K J/m^3 for EW Ag-SPIONs, and 35.2 ± 0.8 K J/m^3 for EW SPIONs.

As mentioned in chapter 2, the magnetization for a collection of non-interacting superparagmagnetic nanoparticles is given by the Langevin function. Therefore, all four magnetization curves were fitted to the Langevin function using OriginLabs software, as shown.
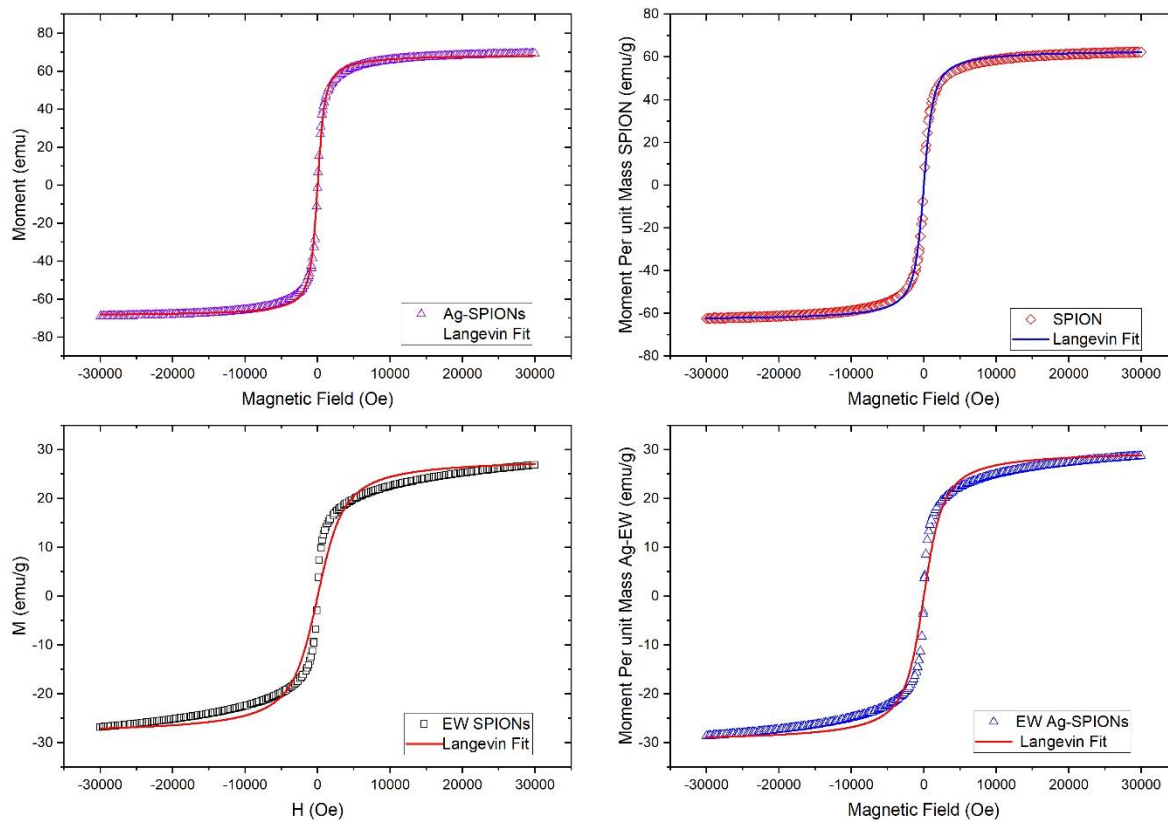
Figure 36: Langevin fit for all samples.

For the Langevin fitting the following expression was used:

$$M = P_1 * [\left(\frac{1}{\tanh{(x * P_2)}} - \frac{1}{P_2}\right)]$$

Which is a reworking of the Langevin function mentioned earlier. Where P_1 is the saturation magnetization and:

$$P_2 = \frac{V}{k_B * T}$$

Where V is the volume, given by:

$$V = \frac{\pi * D^3}{6}$$

Where D is the diameter of the magnetic core, k_B is Boltzmann's constant, and T is the temperature. For Ag-SPIONs the magnetic core diameters were estimated to be 6 ± 2 nm, SPIONs were found to be 5.1 ± 0.6 nm, EW Ag-SPIONs were found to be 4.9 ± 0.5 nm, and EW SPIONs were found to be 4.4 ± 0.4 nm.

In addition to the active magnetic core there are some studies that suggest the existence of a magnetic dead layer on the surface of SPIONs[lvii]. Therefore, a magnetically dead layer was calculated using the expression from a method found in the literature[lviii]:

$$M_s = M_{s,bulk}(1 - \frac{6 * t}{D})$$

Where $M_{s,bulk}$ is the bulk value of magnetization, here 92 emu/g was used, D is the diameter of the particle estimated from XRD, and t is the magnetic dead layer. The magnetic dead layers were found to be 0.38 ± 0.01 nm for Ag-SPIONs, 0.56 ± 0.02 nm for SPIONs, 1.08 ± 0.08 nm for EW Ag-SPIONs, and 0.92 ± 0.04 nm for EW SPIONs.
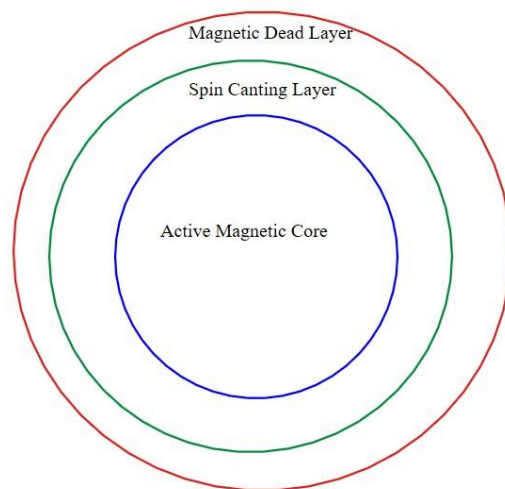
Figure 37: Description of the layers of the SPION.

According to these results it was found that a magnetic core that is less active in the EW samples combined with a larger dead layer has lowered the magnetic response. Additionally, the spin canting region, or not magnetically aligned layer, is the region between these two.

Table 2: The relative sizes of iron oxide only for the four samples.

Sample	XRD Diameter* (nm)	TEM Diameter (nm)	Magnetic Core size (nm)	Dead Layer (nm)
Ag-SPIONs	9.8	11	5.5	0.39
SPIONs	10.8	10	5.1	0.56
EW SPIONs	8.0	7	4.4	0.92
EW Ag-SPIONs	9.6	10	4.9	1.08

*XRD sizes are for Fe_3O_4 only

The Ag-SPIONs have the highest saturation magnetization, which contradicts some of the literature. This is possibly due to the decoration of silver altering the size distribution of SPIONS present. This also is possibly explained by the spin glass freezing phenomenon[lix], which is known to be a dead layer covering the magnetically active core of MNPs. The SPIONs and EW SPIONs were not subjected to higher heats as they were precipitated at ambient temperature. Meanwhile, the Ag-SPIONs and EW Ag-SPIONs underwent high temperature to introduce the silver decoration. This possibly reduced the effect of spin-glass freezing. In the case of the EW SPIONs and EW Ag-SPIONs the literature on egg white properties suggest that heating the substance causes coagulation[lx] at temperatures above 65°C. Given that the EW preparation heated the solution to 80°C, it is likely that coagulation occurred. The literature also suggests that spatial confinement on SPIONs reduces their overall saturation magnetization[lxi]. These two combined suggest that the EW SPIONs and the EW Ag-SPIONs exhibited a reduced saturation magnetization due to coagulation during the synthesis procedure.

4.4 Zero Field Cooling(ZFC)

The ZFC results show that at room temperature, particles above the blocked state and

exhibit super paramagnetic at ambient and physiological temperatures.
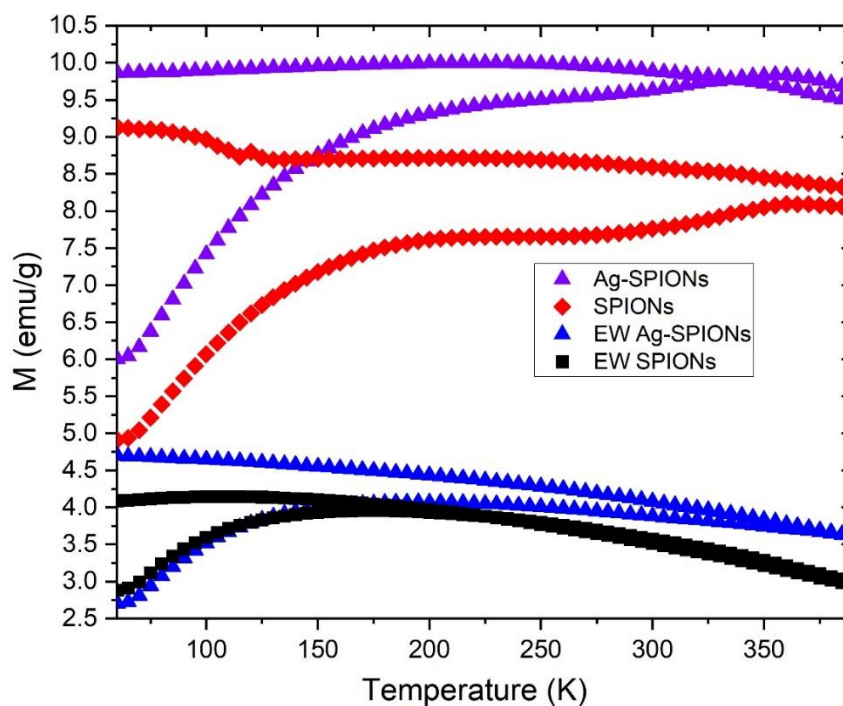
Figure 38: ZFC and FC curves for all four samples. At ambient and physiological temperatures the particles were

found to not be in a blocked state.

4.5 Heating Measurements

The MHT heating profiles of the four samples are shown in the figure below:
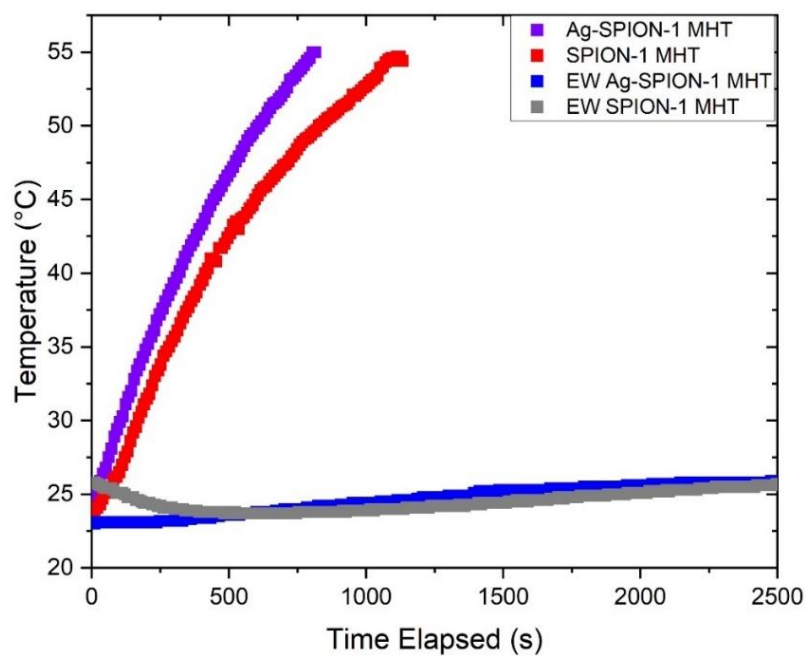
Figure 39: Comparison of MHT on all four samples.

It was observed that Ag-SPION had the highest heating rate of all four samples. With little no heating in the EW samples, owing to their reduced magnetic response. EW Ag-SPIONs were observed to have a higher response than undecorated EW SPIONs.

The heating profile for PHT is shown below:
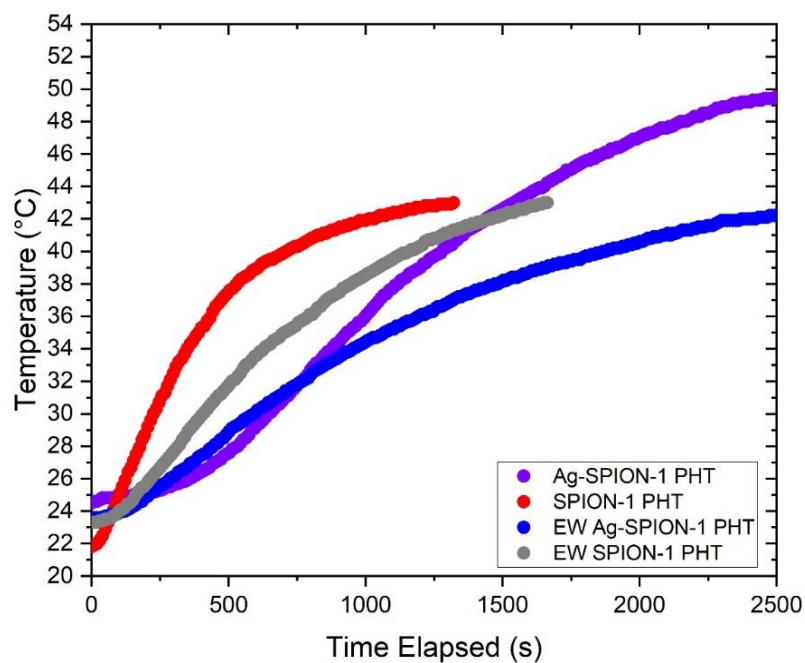
Figure 40: Comparison of PHT for all four samples.

Undecorated SPIONs and EW SPIONs display a higher initial heating rate but Ag-SPION and attains a higher temperature. Both Ag-SPIONs and EW Ag-SPIONs have a slower initial heating rate and higher maximum temperature.

The heating profile for combined heating is shown below:
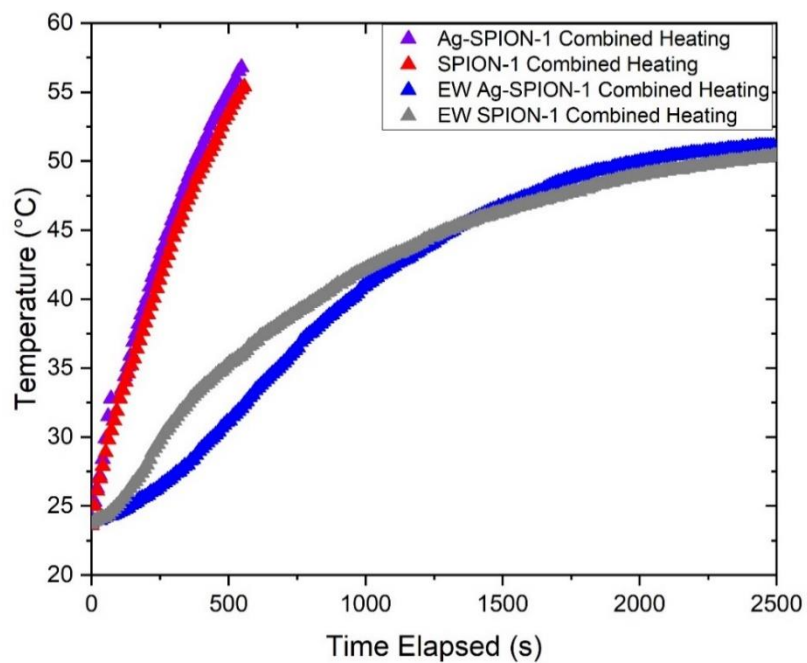
Figure 41: Comparison of combined heating on all four samples.

It was again found that Ag-SPIONs had the highest heating rate, closely followed by SPIONs. Again it was observed that EW SPIONs heated at a higher rate than EW Ag-SPIONs initially. Ultimately, however, the EW Ag-SPIONs attained a higher

temperature. Below are the heating profiles of each sample comparing the heating curves under each heating condition:
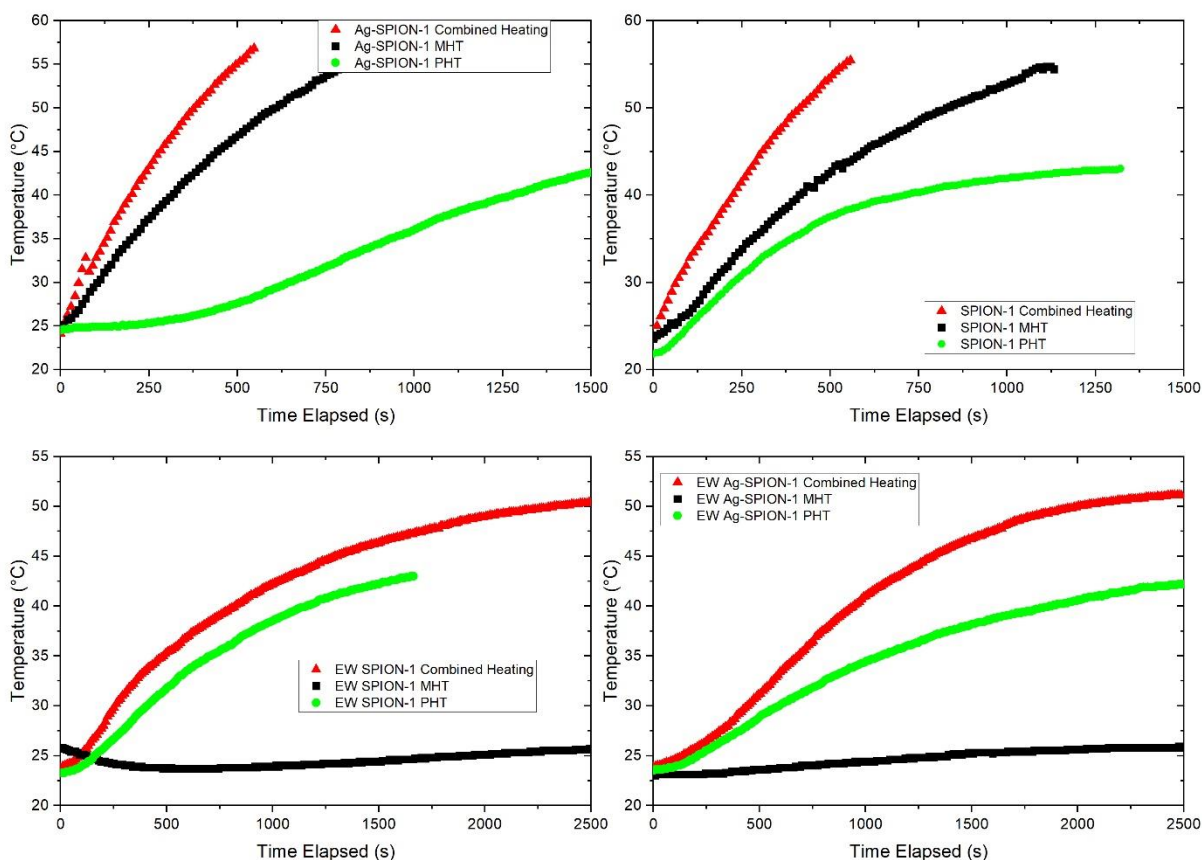
Figure 42: Heating profiles for each sample. Here the three methods of heating are compared to each other on each platform.

As clearly seen from the figures combined heating is the most efficient. For Ag-SPIONs and SPIONs MHT was more efficient than PHT and attained a higher temperature. There is little to no MHT activity for the EW samples. However, there is PHT activity for the EW samples, which is consistent with the conventional samples.

From the calorimetric expression, the temperature dependent SAR values were obtained for each and every heating profile. Using OriginLabs the derivative of each profile was taken and plotted against the temperature.

The next highest were MHT with Ag-SPIONs yielding an initial SAR of 61.5 W/g, SPIONs 54.3 W/g, EW SPIONs 0.9W/g, and EW Ag-SPIONs 2.3 W/g, as shown below:
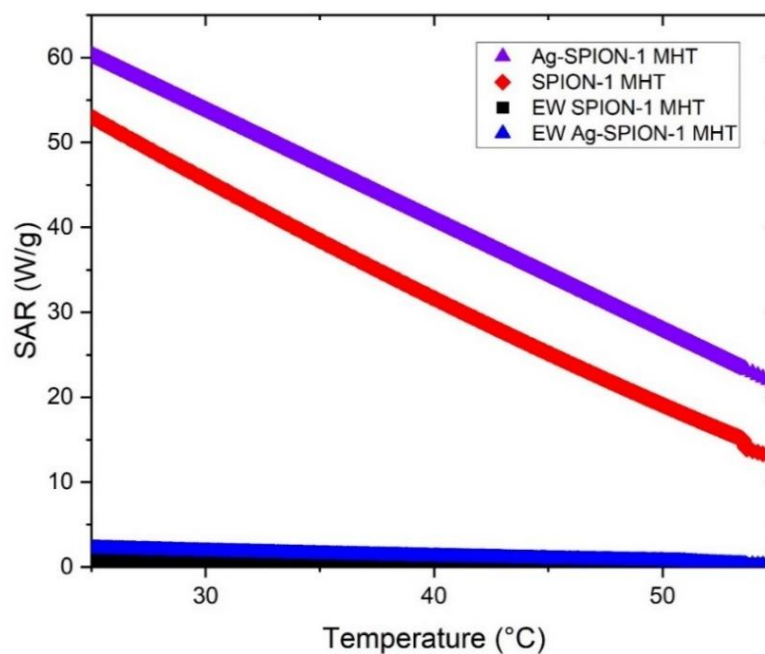
Figure 43: SAR values for all four samples under MHT.

The poor EW response is expected due to the reduced saturation magnetization. For PHT the Ag-SPIONs yielded an initial SAR value of 20.8 W/g, SPIONs 59.3 W/g, EW SPIONs 25.4 W/g, and EW Ag-SPIONs 16.8 W/g, as shown below:
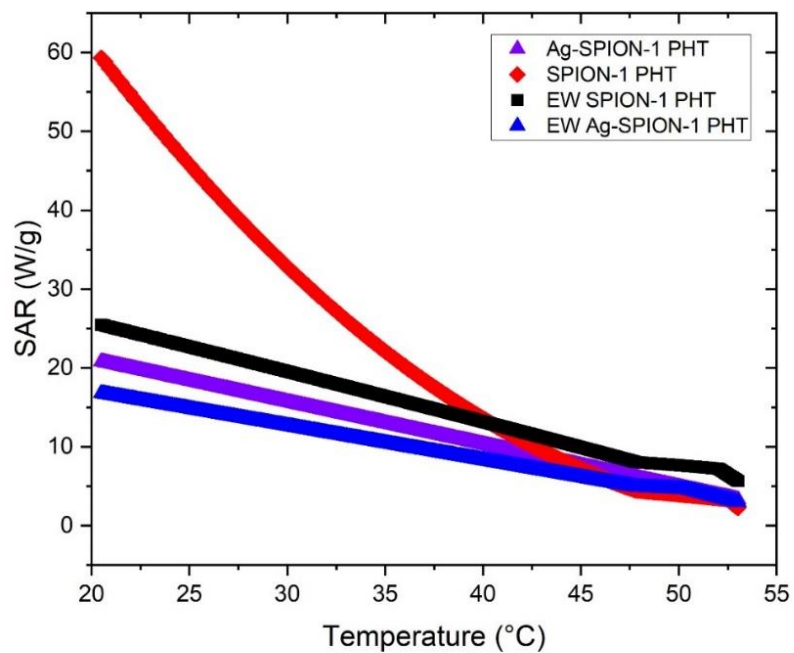
Figure 44: SAR values for all four samples under PHT.

For all heating measurements of all samples, the combined heating had the highest SAR

values, Ag-SPIONs yielding initial SAR values of 90.6 W/g, SPIONs 83.3 W/g, EW

SPIONs 31.5 W/g, and EW Ag-SPIONs 28.1 W/g.
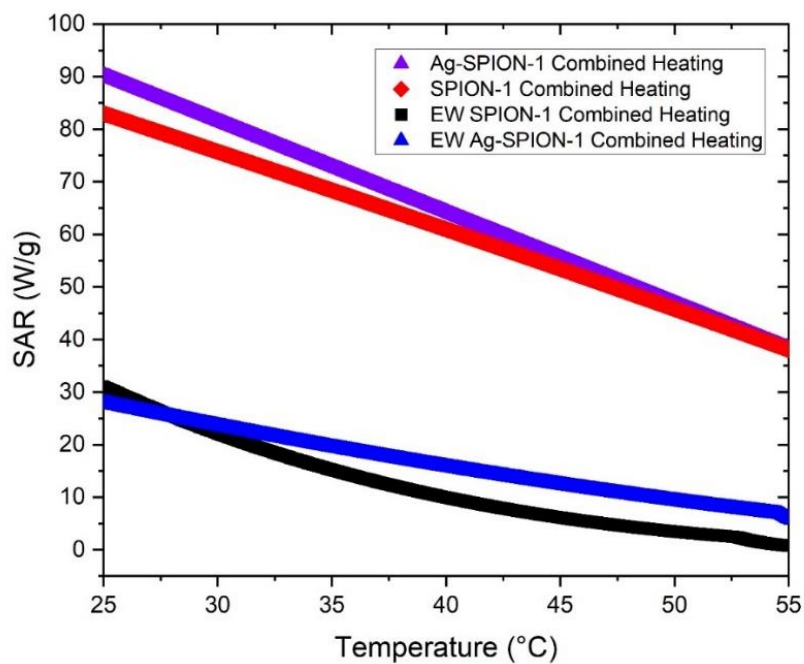
Figure 45: SAR values as a function of temperature for all four samples under combined heating conditions.

This suggests that combined MHT and PHT have the highest heating potential.

Table 3: Initial SAR values. Please see figure 44 for the temperature dependence. In particular for PHT. The contribution of silver from PHT comes as the material heats up.

Sample	MHT SAR(W/g)	PHT SAR(W/g)	Combined SAR(W/g)
Ag-SPIONs	61.5	20.8	90.6
SPIONs	54.3	59.3	83.3
EW SPIONs	0.9	25.4	31.5

EW Ag-SPIONs	2.3	16.8	28.1

When under PHT or combined effects undecorated SPION samples showed a higher initial SAR value, however they plateaued earlier than the silver decorated samples. In the case of PHT, Ag-SPIONs and SPIONs this transition occurs at 43°C, at which point the Ag-SPIONs maintain a higher SAR value per temperature increase. In the case of combined effects, EW Ag-SPIONs and EW SPIONs transition at 30°C, A sharp drop in the undecorated samples occurred while the decorated sample maintained a steady drop in SAR as a function of temperature. It should be noted that SAR values decrease as a result of heating loss capacities of the medium.

According to the literature, usage of AG-NPs for PHT takes place in a physiological range, meaning that the beginning temperature would be higher than ambient. Additionally, there is evidence from other studies that the Plasmonic Resonance redshifts as the particles grow in size or they expand due to thermal expansion[lxii]. Additionally, the effect could also be partially explained by a new resonance forming due to interactions from the bonding of silver and SPION when forming Ag-SPIONs[lxiii]. Combining them would provide a more robust SAR profile through the different temperature ranges. Ag-SPIONs produced the highest SAR value of all four samples, consistently, except in purely PHT, until physiological temperatures were attained. Then the conventional composite maintained a higher SAR and attained a greater temperature.

Chapter 5: Conclusion

In this study three aspects of SPION based applications into cancer treatment were investigated. The first was the magnetic properties of SPIONs upon decorating with silver (Ag). The second was a comparison of MHT, PHT, and combined MHT and PHT and their heating capacity. Finally, the third was comparing synthesis of SPIONs by conventional co-precipitation with a green egg white based approach.

It was found that at a concentration of 5% silver to 95% SPION there was no significant reduction of saturation magnetization. As a result, the effect of decorating SPIONs with silver did not significantly reduce capabilities as an MHT platform. In fact, there was a slight increase in saturation magnetization and MHT performance. Part of this is potentially due to the synthesis method reducing spin glass effects, or size distribution effects of the decoration process.

Combined MHT and PHT clearly provided the highest SAR value, followed by MHT for most configurations. Bare SPIONs possessed a higher initial SAR with a plateau around 42°C, while all configurations with silver exceeded 49°C. The creation of a new resonance frequency and red shift effects due to thermal expansion are the likely cause of this phenomenon. While the SPIONs are an excellent candidate for magneto-photothermal agents, the decoration of silver enhances this capability.

The green synthesis was found to have little to no response to the alternating magnetic field. Plasmonic response was found to be significantly higher, while matching the trend

of conventional synthesis. This is likely the result of coagulation from heat during the synthesis procedure.

Based on the results, a combined platform of Silver decorated SPIONs seem to be a highly viable candidate for heat generation in biomedical applications. Additionally, using egg whites as a capping agent is feasible for less intense heat generation during magneto-photothermal heating.

There is much room for further work. One area would be to vary the power of the laser, studying the laser power dependence of combined MHT and PHT. Additionally, varying the frequency as the peak frequency is higher than 808 nm for both materials. Adjusting the size, shape, and concentration of each material before and during decoration would also be a promising avenue. As for the EW SPIONs and EW Ag-SPIONs studying the effects of denaturing and coagulation on saturation magnetization explicitly would facilitate more precise green synthesis along this procedure.

Bibliography

"808nm 1200mw High Power Focus-Able Near Infrared Laser Module Dot/Line/Crosshair." Accessed April 11, 2023. https://www.civillaser.com/index.php?main_page=product_info&products_id=1275.

Ali, Arbab, Tufail Shah, Rehmat Ullah, Pingfan Zhou, Manlin Guo, Muhammad Ovais, Zhiqiang Tan, and YuKui Rui. "Review on Recent Progress in Magnetic Nanoparticles: Synthesis, Characterization, and Diverse Applications." *Frontiers in Chemistry* 9 (2021). https://www.frontiersin.org/articles/10.3389/fchem.2021.629054.

Ameer, Fathima S., Shilpa Varahagiri, Donald W. Benza, Daniel R. Willett, Yimei Wen, Fenglin Wang, George Chumanov, and Jeffrey N. Anker. "Tuning Localized Surface Plasmon Resonance Wavelengths of Silver Nanoparticles by Mechanical Deformation." *The Journal of Physical Chemistry. C, Nanomaterials and Interfaces* 120, no. 37 (September 22, 2016): 20886–95. https://doi.org/10.1021/acs.jpcc.6b02169.

Angelakeris, M., Zi-An Li, M. Hilgendorff, K. Simeonidis, D. Sakellari, M. Filippousi, H. Tian, et al. "Enhanced Biomedical Heat-Triggered Carriers via Nanomagnetism Tuning in Ferrite-Based Nanoparticles." *Journal of Magnetism and Magnetic Materials* 381 (May 1, 2015): 179–87. https://doi.org/10.1016/j.jmmm.2014.12.069.

Anuthum, Siriporn, Fugo Hasegawa, Chutiparn Lertvachirapaiboon, Kazunari Shinbo, Keizo Kato, Kontad Ounnunkad, and Akira Baba. "Plasmonic Photothermal Properties of Silver Nanoparticle Grating Films." *Physical Chemistry Chemical Physics* 24, no. 11 (March 16, 2022): 7060–67. https://doi.org/10.1039/D1CP05893B.

Arachchige, Maheshika P., Suvra S. Laha, Akshata R. Naik, Kenneth T. Lewis, Ratna Naik, and Bhanu P. Jena. "Functionalized Nanoparticles Enable Tracking the Rapid Entry and Release of Doxorubicin in Human Pancreatic Cancer Cells." *Micron (Oxford, England: 1993)* 92 (January 2017): 25–31. https://doi.org/10.1016/j.micron.2016.10.005.

Arachchige, Maheshika Palihawadana. "Fe3o4 Nanoparticles For Magnetic Hyperthermia And Drug Delivery: Synthesis, Characterization And Cellular Studies," n.d., 141.

Austin, Lauren A., Megan A. Mackey, Erik C. Dreaden, and Mostafa A. El-Sayed. "The Optical, Photothermal, and Facile Surface Chemical Properties of Gold and Silver Nanoparticles in Biodiagnostics, Therapy, and Drug Delivery." *Archives of Toxicology* 88, no. 7 (July 2014): 1391–1417. https://doi.org/10.1007/s00204-014-1245-3.

Campelj, S., D. Makovec, and M. Drofenik. "Preparation and Properties of Water-Based Magnetic Fluids." *Journal of Physics: Condensed Matter* 20, no. 20 (May 2008): 204101. https://doi.org/10.1088/0953-8984/20/20/204101.

Cao, Shao-Wen, Ying-Jie Zhu, Ming-Yan Ma, Liang Li, and Ling Zhang. "Hierarchically Nanostructured Magnetic Hollow Spheres of Fe3O4 and γ-Fe2O3: Preparation and Potential Application in Drug

Delivery." *The Journal of Physical Chemistry C* 112, no. 6 (February 1, 2008): 1851–56. https://doi.org/10.1021/jp077468+.

Chemistry LibreTexts. "11: Linear Response Theory," September 12, 2018. https://chem.libretexts.org/Bookshelves/Physical_and_Theoretical_Chemistry_Textbook_Maps/Time_Dependent_Quantum_Mechanics_and_Spectroscopy_(Tokmakoff)/11%3A_Linear_Response_Theory.

"Chemotherapy Side Effects | American Cancer Society." Accessed April 11, 2023. https://www.cancer.org/treatment/treatments-and-side-effects/treatment-types/chemotherapy/chemotherapy-side-effects.html.

Chettri, Prajwal, Ajay Tripathi, and Archana Tiwari. "Effect of Silver Nanoparticles on Electrical and Magnetic Properties of Reduced Graphene Oxide." *Materials Research Bulletin* 150 (June 1, 2022): 111752. https://doi.org/10.1016/j.materresbull.2022.111752.

Crețu, Bianca Elena-Beatrice, Gianina Dodi, Amin Shavandi, Ioannis Gardikiotis, Ionela Lăcrămioara Șerban, and Vera Balan. "Imaging Constructs: The Rise of Iron Oxide Nanoparticles." *Molecules* 26, no. 11 (January 2021): 3437. https://doi.org/10.3390/molecules26113437.

"Curie Weiss Law – Definition and Limitations." Accessed April 11, 2023. https://www.vedantu.com/physics/curie-weiss-law.

Das, Raja, Natalia Rinaldi-Montes, Javier Alonso Masa, Zakariae Amghouz, Eneko Garaio, Jose Garcia, Pedro Gorria, Jesus Blanco, Manh-Huong Phan, and Hariharan Srikanth. "Boosted Hyperthermia Therapy by Combined AC Magnetic and Photothermal Exposures in Ag/Fe3O4 Nanoflowers." *ACS Applied Materials & Interfaces* 8 (September 2, 2016). https://doi.org/10.1021/acsami.6b09942.

Di Corato, Riccardo, Ana Espinosa, Lenaic Lartigue, Mickael Tharaud, Sophie Chat, Teresa Pellegrino, Christine Ménager, Florence Gazeau, and Claire Wilhelm. "Magnetic Hyperthermia Efficiency in the Cellular Environment for Different Nanoparticle Designs." *Biomaterials* 35, no. 24 (August 1, 2014): 6400–6411. https://doi.org/10.1016/j.biomaterials.2014.04.036.

Dmitruk, Igor, Alexandr Alexeenko, Andriy Kotko, James Vedral, and Anatoliy Pinchuk. "Temperature Dependence of the Surface Plasmon Resonance in Silver Nanoparticles." *Ukrainian Journal of Physics* 57 (February 15, 2012): 266. https://doi.org/10.15407/ujpe57.2.266.

Dong, Jie, Zhenghe Xu, and Steven M. Kuznicki. "Magnetic Multi-Functional Nano Composites for Environmental Applications." *Advanced Functional Materials* 19, no. 8 (2009): 1268–75. https://doi.org/10.1002/adfm.200800982.

Estelrich, Joan, and Maria Antònia Busquets. "Iron Oxide Nanoparticles in Photothermal Therapy." *Molecules* 23, no. 7 (July 2018): 1567. https://doi.org/10.3390/molecules23071567.

Farzin, A., S. Alireza Etesami, Jacob Quint, Adnan Memic, and Ali Tamayol. "Magnetic Nanoparticles in Cancer Therapy and Diagnosis." *Advanced Healthcare Materials* 9, no. 9 (May 2020): e1901058. https://doi.org/10.1002/adhm.201901058.

Fernández-Martín, F., M. Pérez-Mateos, S. Dadashi, C. M. Gómez-Guillén, and P. D. Sanz. "Impact of Magnetic Assisted Freezing in the Physicochemical and Functional Properties of Egg Components. Part 1: Egg White." *Innovative Food Science & Emerging Technologies*, Emerging Technologies with reference to IUFoST, 44 (December 1, 2017): 131–38. https://doi.org/10.1016/j.ifset.2017.07.004.

Fu, Shawei, Yuchun Man, and Fuquan Jia. "Photothermal Effect of Superparamagnetic Fe_3O_4 Nanoparticles Irradiated by Near-Infrared Laser." *Journal of Nanomaterials* 2020 (October 14, 2020): e2832347. https://doi.org/10.1155/2020/2832347.

Gao, Hanwei, Chong Liu, Hoon Eui Jeong, and Peidong Yang. "Plasmon-Enhanced Photocatalytic Activity of Iron Oxide on Gold Nanopillars." *ACS Nano* 6, no. 1 (January 24, 2012): 234–40. https://doi.org/10.1021/nn203457a.

Hajalilou, A., L. P. Ferreira, M. E. Melo Jorge, C. P. Reis, and M. M. Cruz. "Superparamagnetic Ag-Fe3O4 Composites Nanoparticles for Magnetic Fluid Hyperthermia." *Journal of Magnetism and Magnetic Materials* 537 (November 1, 2021): 168242. https://doi.org/10.1016/j.jmmm.2021.168242.

"Hyperthermia to Treat Cancer - NCI." Accessed April 11, 2023. https://www.cancer.gov/about-cancer/treatment/types/hyperthermia.

Ilg, Patrick, and Martin Kröger. "Dynamics of Interacting Magnetic Nanoparticles: Effective Behavior from Competition between Brownian and Néel Relaxation." *Physical Chemistry Chemical Physics* 22, no. 39 (2020): 22244–59. https://doi.org/10.1039/D0CP04377J.

Ivashchenko, Olena, Barbara Peplińska, Jacek Gapiński, Dorota Flak, Marcin Jarek, Karol Załęski, Grzegorz Nowaczyk, Zuzanna Pietralik, and Stefan Jurga. "Silver and Ultrasmall Iron Oxides Nanoparticles in Hydrocolloids: Effect of Magnetic Field and Temperature on Self-Organization." *Scientific Reports* 8, no. 1 (March 6, 2018): 4041. https://doi.org/10.1038/s41598-018-22426-2.

Jain, Prashant K., Yanhong Xiao, Ronald Walsworth, and Adam E. Cohen. "Surface Plasmon Resonance Enhanced Magneto-Optics (SuPREMO): Faraday Rotation Enhancement in Gold-Coated Iron Oxide Nanocrystals." *Nano Letters* 9, no. 4 (April 8, 2009): 1644–50. https://doi.org/10.1021/nl900007k.

Kanwal, Zakia, Muhammad Akram Raza, Saira Riaz, Saher Manzoor, Asima Tayyeb, Imran Sajid, and Shahzad Naseem. "Synthesis and Characterization of Silver Nanoparticle-Decorated Cobalt Nanocomposites (Co@AgNPs) and Their Density-Dependent Antibacterial Activity." *Royal Society Open Science* 6, no. 5 (n.d.): 182135. https://doi.org/10.1098/rsos.182135.

Kim, Dasom, Reeju Amatya, Seungmi Hwang, Sumi Lee, Kyoung Ah Min, and Meong Cheol Shin. "BSA-Silver Nanoparticles: A Potential Multimodal Therapeutics for Conventional and Photothermal Treatment of Skin Cancer." *Pharmaceutics* 13, no. 4 (April 17, 2021): 575. https://doi.org/10.3390/pharmaceutics13040575.

Kobayashi, Takeshi. "Cancer Hyperthermia Using Magnetic Nanoparticles." *Biotechnology Journal* 6, no. 11 (November 2011): 1342–47. https://doi.org/10.1002/biot.201100045.

Kumar, Akshay, Mukesh Kr Chowrasia, Uddyalok Banerjee, and M. K. Banerjee. "Enhancing Structural Stability and Physical Properties of Silver Added Iron-MWCNT Composite Prepared by High Energy Ball Milling and Spark Plasma Sintering." *Diamond and Related Materials* 111 (January 1, 2021): 108228. https://doi.org/10.1016/j.diamond.2020.108228.

Laurent, Sophie, Delphine Forge, Marc Port, Alain Roch, Caroline Robic, Luce Vander Elst, and Robert N. Muller. "Magnetic Iron Oxide Nanoparticles: Synthesis, Stabilization, Vectorization, Physicochemical Characterizations, and Biological Applications." *Chemical Reviews* 108, no. 6 (June 2008): 2064–2110. https://doi.org/10.1021/cr068445e.

Le Trong, Hoa, Kateryna Kiryukhina, Michel Gougeon, Valérie Baco-Carles, Frédéric Courtade, Sophie Dareys, and Philippe Tailhades. "Paramagnetic Behaviour of Silver Nanoparticles Generated by Decomposition of Silver Oxalate." *Solid State Sciences* 69 (July 1, 2017): 44–49. https://doi.org/10.1016/j.solidstatesciences.2017.05.009.

Liu, Xiaoli, Yifan Zhang, Yanyun Wang, Wenjing Zhu, Galong Li, Xiaowei Ma, Yihan Zhang, et al. "Comprehensive Understanding of Magnetic Hyperthermia for Improving Antitumor Therapeutic Efficacy." *Theranostics* 10, no. 8 (February 19, 2020): 3793–3815. https://doi.org/10.7150/thno.40805.

"Magneto-Optical and Catalytic Properties of Fe3O4@HA@Ag Magnetic Nanocomposite | Elsevier Enhanced Reader." Accessed April 6, 2023. https://doi.org/10.1016/j.jmmm.2016.08.037.

Mahmoudi, Morteza, and Vahid Serpooshan. "Silver-Coated Engineered Magnetic Nanoparticles Are Promising for the Success in the Fight against Antibacterial Resistance Threat." *ACS Nano* 6, no. 3 (March 27, 2012): 2656–64. https://doi.org/10.1021/nn300042m.

Manukyan, A., H. Gyulasaryan, A. Kocharian, M. Estiphanos, O. Bernal, and E. Sharoyan. "Ferromagnetism and Giant Paramagnetism of Copper Nanoparticles in Cum/C Nanocomposites." *Journal of Magnetism and Magnetic Materials* 488 (October 15, 2019): 165336. https://doi.org/10.1016/j.jmmm.2019.165336.

Mayo Clinic. "Cancer - Symptoms and Causes." Accessed April 11, 2023. https://www.mayoclinic.org/diseases-conditions/cancer/symptoms-causes/syc-20370588.

Medina-Cruz, David, Bahram Saleh, Ada Vernet-Crua, Alfonso Nieto-Argüello, Diana Lomelí-Marroquín, Lydia Yerid Vélez-Escamilla, Jorge L. Cholula-Díaz, José Miguel García-Martín, and Thomas Webster. "Bimetallic Nanoparticles for Biomedical Applications: A Review." In *Racing for*

the Surface, edited by Bingyun Li, Thomas Fintan Moriarty, Thomas Webster, and Malcolm Xing, 397–434. Cham: Springer International Publishing, 2020. https://doi.org/10.1007/978-3-030-34471-9_16.

Miranda, Renata Rank, Isabella Sampaio, and Valtencir Zucolotto. "Exploring Silver Nanoparticles for Cancer Therapy and Diagnosis." *Colloids and Surfaces B: Biointerfaces* 210 (February 1, 2022): 112254. https://doi.org/10.1016/j.colsurfb.2021.112254.

Mukherjee, Sudip, Lily Liang, and Omid Veiseh. "Recent Advancements of Magnetic Nanomaterials in Cancer Therapy." *Pharmaceutics* 12, no. 2 (February 11, 2020): 147. https://doi.org/10.3390/pharmaceutics12020147.

Muñoz de Escalona, María, Eva Sáez-Fernández, José C. Prados, Consolación Melguizo, and José L. Arias. "Magnetic Solid Lipid Nanoparticles in Hyperthermia against Colon Cancer." *International Journal of Pharmaceutics* 504, no. 1–2 (May 17, 2016): 11–19. https://doi.org/10.1016/j.ijpharm.2016.03.005.

Nasrollahzadeh, Mahmoud, Monireh Atarod, Mohaddeseh Sajjadi, S. Mohammad Sajadi, and Zahra Issaabadi. "Chapter 6 - Plant-Mediated Green Synthesis of Nanostructures: Mechanisms, Characterization, and Applications." In *Interface Science and Technology*, edited by Mahmoud Nasrollahzadeh, S. Mohammad Sajadi, Mohaddeseh Sajjadi, Zahra Issaabadi, and Monireh Atarod, 28:199–322. An Introduction to Green Nanotechnology. Elsevier, 2019. https://doi.org/10.1016/B978-0-12-813586-0.00006-7.

Nnadozie, Ebenezer C., and Peter A. Ajibade. "Multifunctional Magnetic Oxide Nanoparticle (MNP) Core-Shell: Review of Synthesis, Structural Studies and Application for Wastewater Treatment." *Molecules* 25, no. 18 (January 2020): 4110. https://doi.org/10.3390/molecules25184110.

Palihawadana Arachchige, Maheshika. "Fe3o4 Nanoparticles For Magnetic Hyperthermia And Drug Delivery: Synthesis, Characterization And Cellular Studies." *Wayne State University Dissertations*, January 1, 2016. https://digitalcommons.wayne.edu/oa_dissertations/1570.

Park, SungJun, Hye Hun Park, Sung Yeon Kim, Su Jung Kim, Kyoungja Woo, and GwangPyo Ko. "Antiviral Properties of Silver Nanoparticles on a Magnetic Hybrid Colloid." *Applied and Environmental Microbiology* 80, no. 8 (April 2014): 2343–50. https://doi.org/10.1128/AEM.03427-13.

"Peptide-Directed Hierarchical Mineralized Silver Nanocages for Anti-Tumor Photothermal Therapy | ACS Sustainable Chemistry & Engineering." Accessed January 12, 2023. https://pubs.acs.org/doi/pdf/10.1021/acssuschemeng.8b00415.

"Photothermal Conversion - an Overview | ScienceDirect Topics." Accessed October 2, 2022. https://www.sciencedirect.com/topics/earth-and-planetary-sciences/photothermal-conversion.

Prucek, Robert, Jiří Tuček, Martina Kilianová, Aleš Panáček, Libor Kvítek, Jan Filip, Milan Kolář, Kateřina Tománková, and Radek Zbořil. "The Targeted Antibacterial and Antifungal Properties of

Magnetic Nanocomposite of Iron Oxide and Silver Nanoparticles." *Biomaterials* 32, no. 21 (July 1, 2011): 4704–13. https://doi.org/10.1016/j.biomaterials.2011.03.039.

Roca, Alejandro G., Lucía Gutiérrez, Helena Gavilán, Maria Eugênia Fortes Brollo, Sabino Veintemillas-Verdaguer, and María del Puerto Morales. "Design Strategies for Shape-Controlled Magnetic Iron Oxide Nanoparticles." *Advanced Drug Delivery Reviews*, Physically-triggered nanosystems for therapy and diagnosis, 138 (January 1, 2019): 68–104. https://doi.org/10.1016/j.addr.2018.12.008.

Rodríguez-Luccioni, Héctor L, Magda Latorre-Esteves, Janet Méndez-Vega, Orlando Soto, Ana R Rodríguez, Carlos Rinaldi, and Madeline Torres-Lugo. "Enhanced Reduction in Cell Viability by Hyperthermia Induced by Magnetic Nanoparticles." *International Journal of Nanomedicine* 6 (2011): 373–80. https://doi.org/10.2147/IJN.S14613.

Sadat, M. E., Ronak Patel, Jason Sookoor, Sergey L. Bud'ko, Rodney C. Ewing, Jiaming Zhang, Hong Xu, et al. "Effect of Spatial Confinement on Magnetic Hyperthermia via Dipolar Interactions in Fe3O4 Nanoparticles for Biomedical Applications." *Materials Science and Engineering: C* 42 (September 1, 2014): 52–63. https://doi.org/10.1016/j.msec.2014.04.064.

Salata, OV. "Applications of Nanoparticles in Biology and Medicine." *Journal of Nanobiotechnology* 2, no. 1 (April 30, 2004): 3. https://doi.org/10.1186/1477-3155-2-3.

Samrot, Antony V., Chamarthy Sai Sahithya, Jenifer Selvarani A, Sajna Keeyari Purayil, and Paulraj Ponnaiah. "A Review on Synthesis, Characterization and Potential Biological Applications of Superparamagnetic Iron Oxide Nanoparticles." *Current Research in Green and Sustainable Chemistry* 4 (January 1, 2021): 100042. https://doi.org/10.1016/j.crgsc.2020.100042.

Sawicki, M, W Stefanowicz, and A Ney. "Sensitive SQUID Magnetometry for Studying Nanomagnetism." *Semiconductor Science and Technology* 26, no. 6 (June 8, 2011): 064006. https://doi.org/10.1088/0268-1242/26/6/064006.

Seideman, W.E., O.J. Cotterill, and E.M. Funk. "Factors Affecting Heat Coagulation of Egg White." *Poultry Science* 42, no. 2 (March 1963): 406–17. https://doi.org/10.3382/ps.0420406.

Shen, Shun, Sheng Wang, Rui Zheng, Xiaoyan Zhu, Xinguo Jiang, Deliang Fu, and Wuli Yang. "Magnetic Nanoparticle Clusters for Photothermal Therapy with Near-Infrared Irradiation." *Biomaterials* 39 (January 2015): 67–74. https://doi.org/10.1016/j.biomaterials.2014.10.064.

Shivanna, Anilkumar Thaghalli, Banendu Sunder Dash, and Jyh-Ping Chen. "Functionalized Magnetic Nanoparticles for Alternating Magnetic Field- or Near Infrared Light-Induced Cancer Therapies." *Micromachines* 13, no. 8 (August 8, 2022): 1279. https://doi.org/10.3390/mi13081279.

"Side Effects of Radiation Therapy | Radiation Effects on Body." Accessed April 11, 2023. https://www.cancer.org/treatment/treatments-and-side-effects/treatment-types/radiation/effects-on-different-parts-of-body.html.

"The Magnetization of Pure Iron and Nickel." *Proceedings of the Royal Society of London. A. Mathematical and Physical Sciences*, March 9, 1971. https://doi.org/10.1098/rspa.1971.0044.

Venkatesan, Kaliyamoorthy, Dhanakotti Rajan Babu, Mane Prabhu Kavya Bai, Ravi Supriya, Radhakrishnan Vidya, Saminathan Madeswaran, Pandurangan Anandan, Mukannan Arivanandhan, and Yasuhiro Hayakawa. "Structural and Magnetic Properties of Cobalt-Doped Iron Oxide Nanoparticles Prepared by Solution Combustion Method for Biomedical Applications." *International Journal of Nanomedicine* 10, no. Supplement 1 Challenges in biomaterials research (October 1, 2015): 189–98. https://doi.org/10.2147/IJN.S82210.

Weir, Hannah K. "Cancer Incidence Projections in the United States Between 2015 and 2050." *Preventing Chronic Disease* 18 (2021). https://doi.org/10.5888/pcd18.210006.

Xie, Wensheng, Zhenhu Guo, Fei Gao, Qin Gao, Dan Wang, Bor-shuang Liaw, Qiang Cai, Xiaodan Sun, Xiumei Wang, and Lingyun Zhao. "Shape-, Size- and Structure-Controlled Synthesis and Biocompatibility of Iron Oxide Nanoparticles for Magnetic Theranostics." *Theranostics* 8, no. 12 (May 11, 2018): 3284–3307. https://doi.org/10.7150/thno.25220.

Yamamoto, T. A., R. D. Shull, and H. W. Hahn. "Magnetization of Iron-Oxide/Silver Nanocomposite by Inert Gas Condensation." *Nanostructured Materials* 9, no. 1 (January 1, 1997): 539–42. https://doi.org/10.1016/S0965-9773(97)00119-0.

Yeşilot, Şükriye, and Çiğdem Aydın Acar. "Silver Nanoparticles; a New Hope in Cancer Therapy?" *Eastern Journal Of Medicine* 24, no. 1 (2019): 111–16. https://doi.org/10.5505/ejm.2019.66487.

Yuan, Muzhaozi, Tian-Hao Yan, Jialuo Li, Zhifeng Xiao, Yu Fang, Ya Wang, Hong-Cai Zhou, and Jean-Philippe Pellois. "Superparamagnetic Iron Oxide-Gold Nanoparticles Conjugated with Porous Coordination Cages: Towards Controlled Drug Release for Non-Invasive Neuroregeneration." *Nanomedicine: Nanotechnology, Biology, and Medicine* 35 (July 2021): 102392. https://doi.org/10.1016/j.nano.2021.102392.

Zhang, Huan, Xiao Li Liu, Yi Fan Zhang, Fei Gao, Ga Long Li, Yuan He, Ming Li Peng, and Hai Ming Fan. "Magnetic Nanoparticles Based Cancer Therapy: Current Status and Applications." *Science China. Life Sciences* 61, no. 4 (April 2018): 400–414. https://doi.org/10.1007/s11427-017-9271-1.

Zhu, Jiahua, Suying Wei, Minjiao Chen, Hongbo Gu, Sowjanya B. Rapole, Sameer Pallavkar, Thomas C. Ho, Jack Hopper, and Zhanhu Guo. "Magnetic Nanocomposites for Environmental Remediation." *Advanced Powder Technology* 24, no. 2 (March 2013): 459–67. https://doi.org/10.1016/j.apt.2012.10.012.

[i] https://www.cdc.gov/pcd/issues/2021/21_0006.htm, 2/15/2023

[ii] https://www.mayoclinic.org/diseases-conditions/cancer/symptoms-causes/syc-20370588, 2/15/2023

[iii] https://www.freepik.com/free-vector/cancer-development-process-infographic_24785346.htm

[iv iv] https://www.cancer.org/treatment/treatments-and-side-effects/treatment-types/chemotherapy/chemotherapy-side-effects.html [1]

[v] https://www.cancer.org/treatment/treatments-and-side-effects/treatment-types/radiation/effects-on-different-parts-of-body.html

[vi] OV Salata, "Applications of Nanoparticles in Biology and Medicine," Journal of Nanobiotechnology 2, no. 1 (April 30, 2004): 3, https://doi.org/10.1186/1477-3155-2-3.

[vii] https://www.researchgate.net/publication/330292807_Combination_of_Cell-Penetrating_Peptides_with_Nanoparticles_for_Therapeutic_Application_A_Review/figures?lo=1

[viii] Sudip Mukherjee, Lily Liang, and Omid Veiseh, "Recent Advancements of Magnetic Nanomaterials in Cancer Therapy," Pharmaceutics 12, no. 2 (February 11, 2020): 147, https://doi.org/10.3390/pharmaceutics12020147.

[ix] https://convertio.co/download/cd747febd1d8da06cc1a78a5dde24f462a267f/

[x] Mukherjee, Liang, and Veiseh, "Recent Advancements of Magnetic Nanomaterials in Cancer Therapy."

[xi] https://www.researchgate.net/figure/Some-of-the-important-applications-of-SPIONs_fig1_341192702

[xii] https://www.mdpi.com/1422-0067/14/8/15977#

[xiii] https://www.vedantu.com/physics/curie-weiss-law

[xiv] https://www.mdpi.com/1422-0067/14/8/15977#

[xv] https://chem.libretexts.org/Bookshelves/Physical_and_Theoretical_Chemistry_Textbook_Maps/Time_Dependent_Quantum_Mechanics_and_Spectroscopy_(Tokmakoff)/11%3A_Linear_Response_Theory#:~:text=Linear%20response%20theory%20is%20the,toward%20equilibrium%20under%20perturbative%20conditions.&text=We%20will%20use%20linear%20response,deal%20with%20a%20nonequilibrium%20system.

[xvi] Patrick Ilg and Martin Kröger, "Dynamics of Interacting Magnetic Nanoparticles: Effective Behavior from Competition between Brownian and Néel Relaxation," Physical Chemistry Chemical Physics 22, no. 39 (2020): 22244–59, https://doi.org/10.1039/D0CP04377J.

[xvii] Curley SA, Palalon F, Sanders KE, Koshkina NV. The effects of non-invasive radiofrequency treatment and hyperthermia on malignant and nonmalignant cells. Int J Environ Res Public Health. 2014 Sep 3;11(9):9142-53. doi: 10.3390/ijerph110909142. PMID: 25192147; PMCID: PMC4199010.

[xviii] Héctor L Rodríguez-Luccioni et al., "Enhanced Reduction in Cell Viability by Hyperthermia Induced by Magnetic Nanoparticles," International Journal of Nanomedicine 6 (2011): 373–80, https://doi.org/10.2147/IJN.S14613.

xix Rodríguez-Luccioni et al.; Huan Zhang et al., "Magnetic Nanoparticles Based Cancer Therapy: Current Status and Applications," Science China. Life Sciences 61, no. 4 (April 2018): 400–414, https://doi.org/10.1007/s11427-017-9271-1.

xx https://www.mdpi.com/2312-7481/6/4/68#

xxi Takeshi Kobayashi, "Cancer Hyperthermia Using Magnetic Nanoparticles," Biotechnology Journal 6, no. 11 (November 2011): 1342–47, https://doi.org/10.1002/biot.201100045; "Hyperthermia to Treat Cancer - NCI," accessed April 11, 2023, https://www.cancer.gov/about-cancer/treatment/types/hyperthermia.
xxii Joan Estelrich and Maria Antònia Busquets, "Iron Oxide Nanoparticles in Photothermal Therapy," Molecules 23, no. 7 (July 2018): 1567, https://doi.org/10.3390/molecules23071567.
xxiii Griffiths, David. Introduction of Quantum Mechanics. : Prentice Hall, Inc., 1995.

xxiv https://pubs.rsc.org/en/content/articlelanding/2022/cp/d1cp05893b

xxv https://www.sciencedirect.com/topics/earth-and-planetary-sciences/photothermal-conversion

xxvi Austin et al., "The Optical, Photothermal, and Facile Surface Chemical Properties of Gold and Silver Nanoparticles in Biodiagnostics, Therapy, and Drug Delivery."

xxvii Yeşilot and Aydın Acar, "Silver Nanoparticles; a New Hope in Cancer Therapy?"

xxviii https://www.sciencedirect.com/science/article/abs/pii/S0927776521007001

xxix Shawei Fu, Yuchun Man, and Fuquan Jia, "Photothermal Effect of Superparamagnetic Fe_3O_4 Nanoparticles Irradiated by Near-Infrared Laser," Journal of Nanomaterials 2020 (October 14, 2020): e2832347, https://doi.org/10.1155/2020/2832347.
xxx Xiaoli Liu et al., "Comprehensive Understanding of Magnetic Hyperthermia for Improving Antitumor Therapeutic Efficacy," Theranostics 10, no. 8 (February 19, 2020): 3793–3815, https://doi.org/10.7150/thno.40805.
xxxi Liu et al.
xxxii Liu et al.
xxxiii Mukherjee, Liang, and Veiseh, "Recent Advancements of Magnetic Nanomaterials in Cancer Therapy."
xxxiv Di Corato et al., "Magnetic Hyperthermia Efficiency in the Cellular Environment for Different Nanoparticle Designs."
xxxv Alejandro G. Roca et al., "Design Strategies for Shape-Controlled Magnetic Iron Oxide Nanoparticles," Advanced Drug Delivery Reviews, Physically-triggered nanosystems for therapy and diagnosis, 138 (January 1, 2019): 68–104, https://doi.org/10.1016/j.addr.2018.12.008.
xxxvi Kaliyamoorthy Venkatesan et al., "Structural and Magnetic Properties of Cobalt-Doped Iron Oxide Nanoparticles Prepared by Solution Combustion Method for Biomedical Applications," International Journal of Nanomedicine 10, no. Supplement 1 Challenges in biomaterials research (October 1, 2015): 189–98, https://doi.org/10.2147/IJN.S82210; Mukherjee, Liang, and Veiseh, "Recent Advancements of Magnetic Nanomaterials in Cancer Therapy."

[xxxvii] David Medina-Cruz et al., "Bimetallic Nanoparticles for Biomedical Applications: A Review," in Racing for the Surface, ed. Bingyun Li et al. (Cham: Springer International Publishing, 2020), 397–434, https://doi.org/10.1007/978-3-030-34471-9_16.

[xxxviii] A. Hajalilou et al., "Superparamagnetic Ag-Fe3O4 Composites Nanoparticles for Magnetic Fluid Hyperthermia," Journal of Magnetism and Magnetic Materials 537 (November 1, 2021): 168242, https://doi.org/10.1016/j.jmmm.2021.168242; Muzhaozi Yuan et al., "Superparamagnetic Iron Oxide-Gold Nanoparticles Conjugated with Porous Coordination Cages: Towards Controlled Drug Release for Non-Invasive Neuroregeneration," Nanomedicine: Nanotechnology, Biology, and Medicine 35 (July 2021): 102392, https://doi.org/10.1016/j.nano.2021.102392; Raja Das et al., "Boosted Hyperthermia Therapy by Combined AC Magnetic and Photothermal Exposures in Ag/Fe3O4 Nanoflowers," ACS Applied Materials & Interfaces 8 (September 2, 2016), https://doi.org/10.1021/acsami.6b09942; Morteza Mahmoudi and Vahid Serpooshan, "Silver-Coated Engineered Magnetic Nanoparticles Are Promising for the Success in the Fight against Antibacterial Resistance Threat," ACS Nano 6, no. 3 (March 27, 2012): 2656–64, https://doi.org/10.1021/nn300042m; Robert Prucek et al., "The Targeted Antibacterial and Antifungal Properties of Magnetic Nanocomposite of Iron Oxide and Silver Nanoparticles," Biomaterials 32, no. 21 (July 1, 2011): 4704–13, https://doi.org/10.1016/j.biomaterials.2011.03.039; Olena Ivashchenko et al., "Silver and Ultrasmall Iron Oxides Nanoparticles in Hydrocolloids: Effect of Magnetic Field and Temperature on Self-Organization," Scientific Reports 8, no. 1 (March 6, 2018): 4041, https://doi.org/10.1038/s41598-018-22426-2; "Magneto-Optical and Catalytic Properties of Fe3O4@HA@Ag Magnetic Nanocomposite | Elsevier Enhanced Reader," accessed April 6, 2023, https://doi.org/10.1016/j.jmmm.2016.08.037; SungJun Park et al., "Antiviral Properties of Silver Nanoparticles on a Magnetic Hybrid Colloid," Applied and Environmental Microbiology 80, no. 8 (April 2014): 2343–50, https://doi.org/10.1128/AEM.03427-13.

[xxxix] Antony V. Samrot et al., "A Review on Synthesis, Characterization and Potential Biological Applications of Superparamagnetic Iron Oxide Nanoparticles," Current Research in Green and Sustainable Chemistry 4 (January 1, 2021): 100042, https://doi.org/10.1016/j.crgsc.2020.100042.

[xl] Bianca Elena-Beatrice Crețu et al., "Imaging Constructs: The Rise of Iron Oxide Nanoparticles," Molecules 26, no. 11 (January 2021): 3437, https://doi.org/10.3390/molecules26113437.

[xli] Hajalilou et al., "Superparamagnetic Ag-Fe3O4 Composites Nanoparticles for Magnetic Fluid Hyperthermia."

[xlii] S. Campelj, D. Makovec, and M. Drofenik, "Preparation and Properties of Water-Based Magnetic Fluids," Journal of Physics: Condensed Matter 20, no. 20 (May 2008): 204101, https://doi.org/10.1088/0953-8984/20/20/204101.

[xliii] Hajalilou et al., "Superparamagnetic Ag-Fe3O4 Composites Nanoparticles for Magnetic Fluid Hyperthermia."

[xliv] Maheshika Palihawadana Arachchige, "Fe3o4 Nanoparticles For Magnetic Hyperthermia And Drug Delivery: Synthesis, Characterization And Cellular Studies," n.d., 141.

[xlv] Arachchige.

[xlvi] S. Laurent, D. Forge, M. Port, A. Roch, C. Robic, L. Vander Elst, R.N. Muller, Chemical Reviews 108 (2008) 2064.

[xlvii] O. Veiseh, J. Gunn, M. Zhang, Advanced drug delivery reviews 62 (2010) 284.

[xlviii] https://pubs.usgs.gov/of/2001/of01-041/htmldocs/images/beam.jpg

[xlix] Arachchige, "Fe3o4 Nanoparticles For Magnetic Hyperthermia And Drug Delivery: Synthesis, Characterization And Cellular Studies."

[l] Mahmoud Nasrollahzadeh et al., "Chapter 6 - Plant-Mediated Green Synthesis of Nanostructures: Mechanisms, Characterization, and Applications," in Interface Science and Technology, ed. Mahmoud Nasrollahzadeh et al., vol. 28, An Introduction to Green Nanotechnology (Elsevier, 2019), 199–322, https://doi.org/10.1016/B978-0-12-813586-0.00006-7.

[li] https://en.wikipedia.org/wiki/Vibrating-sample_magnetometer#/media/File:VSM_en.svg

[lii] https://en.wikipedia.org/wiki/Vibrating-sample_magnetometer#/media/File:A_Vibrating_Sample_Magnetometer_(VSM).jpg

[liii] https://www.civillaser.com/index.php?main_page=product_info&products_id=1275

[liv] Griffiths, David. Introduction of Quantum Mechanics. : Prentice Hall, Inc., 1995.

[lv] "Magneto-Optical and Catalytic Properties of Fe3O4@HA@Ag Magnetic Nanocomposite | Elsevier Enhanced Reader."

[lvi] "Magneto-Optical and Catalytic Properties of Fe3O4@HA@Ag Magnetic Nanocomposite | Elsevier Enhanced Reader."

[lvii] "Magneto-Optical and Catalytic Properties of Fe3O4@HA@Ag Magnetic Nanocomposite | Elsevier Enhanced Reader."

[lviii] "Magneto-Optical and Catalytic Properties of Fe3O4@HA@Ag Magnetic Nanocomposite | Elsevier Enhanced Reader."

[lix] T. A. Yamamoto, R. D. Shull, and H. W. Hahn, "Magnetization of Iron-Oxide/Silver Nanocomposite by Inert Gas Condensation," Nanostructured Materials 9, no. 1 (January 1, 1997): 539–42, https://doi.org/10.1016/S0965-9773(97)00119-0.

[lx] W.E. Seideman, O.J. Cotterill, and E.M. Funk, "Factors Affecting Heat Coagulation of Egg White," Poultry Science 42, no. 2 (March 1963): 406–17, https://doi.org/10.3382/ps.0420406.

[lxi] M. E. Sadat et al., "Effect of Spatial Confinement on Magnetic Hyperthermia via Dipolar Interactions in Fe3O4 Nanoparticles for Biomedical Applications," Materials Science and Engineering: C 42 (September 1, 2014): 52–63, https://doi.org/10.1016/j.msec.2014.04.064.

[lxii] Igor Dmitruk et al., "Temperature Dependence of the Surface Plasmon Resonance in Silver Nanoparticles," Ukrainian Journal of Physics 57 (February 15, 2012): 266, https://doi.org/10.15407/ujpe57.2.266.

[lxiii] Prashant K. Jain et al., "Surface Plasmon Resonance Enhanced Magneto-Optics (SuPREMO): Faraday Rotation Enhancement in Gold-Coated Iron Oxide Nanocrystals," Nano Letters 9, no. 4 (April 8, 2009): 1644–50, https://doi.org/10.1021/nl900007k.